Studies on the Pharmacological Effects of Panitumumab

January 2020

Yuji BABA

Studies on the Pharmacological Effects of Panitumumab

A Dissertation Submitted to

the Graduate School of Life and Environmental Sciences,

the University of Tsukuba

in Partial Fulfillment of the Requirements

for the Degree of Doctor of Philosophy in Biological Science

（Doctoral Program in Biological Sciences）

Yuji BABA

Table of Contents

Abstract 1

Abbreviations 4

General Introduction 6

Chapter 1 12

Abstract 13

Introduction 15

Materials and Methods 17

Results 26

Discussion 33

Tables and Figures 37

Chapter 2 54

Abstract 55

Introduction 57

Materials and Methods 60

Results 66

Discussion 70

Tables and Figures 74

General Discussion 85

Acknowledgements 88

References 89

Abstract

Panitumumab is a monoclonal antibody raised against the human epidermal growth factor receptor (EGFR). The EGFR is highly expressed in a number of solid tumors and its expression correlates with tumor progression and resistance to chemotherapy. Drugs targeting the EGFR have demonstrated some success (increased progression-free and survival period) in patients with colorectal cancer (CRC). Panitumumab has been approved in many countries since it was first approved in the United States in 2006 for the indication of CRC. However, there are few reports that have evaluated the effects of combination treatments or variation in the sequential order of drug administration for treatment of CRC.

In the first chapter of this thesis, I evaluated the antitumor activity of a combination of panitumumab (an anti-EGFR antibody) and TAS-102 [a nucleoside antitumor agent consisting of trifluridine (FTD) and tipiracil] in a mouse model transplanted with human CRC cells. The combination treatment yielded a stronger antitumor effect than either single agent. Next, I evaluated the effect of FTD on EGFR phosphorylation and found that FTD induced serine/threonine phosphorylation of the EGFR. Additionally, I found that FTD induced the activation of ERK/AKT/STAT3, which are EGFR downstream pathways involved in cancer malignancy. Interestingly, the FTD -mediated activation of the ERK/AKT/STAT3 pathways was

suppressed by adding panitumumab. Thus, panitumumab suppresses malignant cancer determinants activated by FTD. From these results, I hypothesize that panitumumab inhibits tyrosine phosphorylation induced by endogenous ligands, thereby inhibiting FTD -mediated induction of serine/threonine phosphorylation of the EGFR and ERK/AKT/STAT3 activation. The newly discovered pharmacological action mediated by panitumumab may be able to solve the problems associated with TAS-102.

In the second chapter of this dissertation, I studied the antitumor effects of varying the sequential order of administration of panitumumab and bevacizumab (an anti-VEGF antibody) in a mouse model transplanted with human CRC cells. Sequential administration of panitumumab followed by bevacizumab (PB) showed a stronger tendency to inhibit tumor growth compared to treatment with bevacizumab followed by panitumumab (BP). Next, I analyzed the phosphorylation status of ephrin type-A receptor 2 (EPHA2), which is a malignant cancer determinant. EPHA2 phosphorylation was significantly decreased in the PB group compared to the control group. I also found that the expression of genes involved in lipogenesis and hypoxia, which are malignant cancer determinants, were significantly decreased in the PB group compared to the control group. These results revealed distinct pharmacological actions of panitumumab and bevacizumab based on their sequential order of administration.

Taken together, these studies demonstrated a novel pharmacological action of panitumumab by evaluating the pharmacological effects of panitumumab/TAS-102 combination therapy or the panitumumab/bevacizumab sequential order of administration.

Abbreviations

AKT	protein kinase B
BB	bevacizumab-bevacizumab
BP	bevacizumab followed by panitumumab
BrdU	5-bromo-2'-deoxyuridine
CA9	carbonic anhydrase 9
CRC	colorectal cancer
DEGs	differentially expressed genes
DMSO	dimethyl sulfoxide
EGFR	epidermal growth factor receptor
EPHA2	ephrin type-A receptor 2
ERK	extracellular signal-regulated kinase
FASN	fatty acid synthase
FBS	fetal bovine serum
FOLFIRI	fluorouracil, leucovorin, and irinotecan
FOLFOX	fluorouracil, leucovorin, and oxaliplatin
FTD	trifluridine
FU	fluorouracil
GAPDH	glyceraldehyde 3-phosphate dehydrogenase
GR	growth rate
GTPase	guanosine triphosphate hydrolase
HIF	hypoxia-inducible factor
HMGCR	HMG-CoA reductase
HR	hazard ratio
IGF2R	insulin-like growth factor 2 receptor
KRAS	Kirsten rat sarcoma viral oncogene homolog
LC/MS/MS	liquid chromatography-tandem mass spectrometry
LSS	lanosterol synthase
MAPK	mitogen-activated protein kinase
mCRC	metastatic colorectal cancer
MeCN	acetonitril
MEK	mitogen-activated protein kinase kinase

MP	monophosphate
MS	mass spectrometry
MVD	mevalonate disphosphate decarboxylase
OS	overall survival
PB	panitumumab followed by bevacizumab
PDX	patient-derived colon tumor xenograft
pEPHA2	phosphorylated EPHA2
PFS	progression-free survival
PI3K	phosphatidylinositol 3-kinase
pRSK	phosphorylated RSK
qRT-PCR	quantitative realtime polymerase chain reaction
RAF	rapidly accelerated fibrosarcoma kinase
RAS	rat sarcoma GTPase
RSK	ribosomal S6 kinase
SCID	C.B17/Icr-scid/scid Jcl
SDS	sodium dodecyl sulfate
SILAC	stable isotope labeling with amino acids in cell culture
STAT	signal transducer and activator of transcription
TEAB	triethylammonium bicarbonate
TGFBI	transforming growth factor-β induced protein
TNF	tumor necrosis factor
TP	triphosphate
TPI	tipiracil hydrochloride
TS	thymidylate synthase
VEGF	vascular endothelial growth factor
WT	wild-type

General Introduction

Colorectal cancer (CRC) is the fourth most commonly diagnosed cancer and the fifth-leading cause of cancer-related death worldwide[1]. The number of CRC-induced deaths is expected to rise by 60% when comparing CRC deaths in 2013 to the projection of CRC deaths 2035. This increase is mainly due to population growth and ageing[2]. Approximately 25% of CRC patients present metastatic disease (mCRC) at diagnosis, and almost 50% will subsequently develop metastases[3]. Single-drug treatment strategies for mCRC patients are limited, but recent efforts to improve survival outcomes among these patients have focused on the combination of conventional chemotherapies with agents targeting biological pathways that are pivotal for cancer pathogenesis. Patients with advanced and unresectable CRC may be eligible for multiple lines of treatment. Presently, there are 13 therapeutic agents used for the treatment of mCRC in Japan, including 5-fluorouracil (5-FU), tegafur/uracil (UFT), tegafur/gimeracil/oteracil (S-1), irinotecan, capecitabine, oxaliplatin, trifluridine/tipiracil (TAS-102), bevacizumab, cetuximab, panitumumab, regorafenib, ramucirumab and aflibercept. Three major chemotherapeutic agents (5-FU, irinotecan and oxaliplatin), two anti-epidermal growth factor receptor (anti-EGFR) antibodies (panitumumab and cetuximab) and an anti-vascular endothelial growth factor (anti-VEGF) antibody (bevacizumab) have exihibited well-demonstrated clinical efficacy for the treatment of mCRC[4,5].

The current standard of care for mCRC involves a backbone of cytotoxic chemotherapy, using regimens such as 5-FU, leucovorin, and irinotecan (FOLFIRI) and 5-FU, leucovorin, and oxaliplatin (FOLFOX) combined with targeted agents[3,6]. The use of these chemotherapeutic regimens in combination with an anti- EGFR antibody, such as panitumumab or cetuximab, or the anti-VEGF antibody bevacizumab improve survival compared with chemotherapy alone[7-12].

Mechanistically, both panitumumab and cetuximab competitively inhibit endogenous ligand binding, and thereby suppress the subsequent activation of the EGFR, a member of the human epidermal growth factor receptor–ErbB (ERBB) family of receptor tyrosine kinases. EGFR tyrosine kinase activation stimulates key processes involved in tumor growth and progressoin via activation of the following downstream signaling pathways, rat sarcoma GTPase (RAS) /rapidly accelerated fibrosarcoma kinase (RAF) /mitogen-activated protein kinase kinase (MEK) /extracellular signal-regulated kinase (ERK), phosphatidylinositol 3–kinase (PI3K)- protein kinase B (AKT), and signal transducer and activator of transcription (STAT) (Fig. 1)[13-15]. One of the key downstream targets of the RAS/RAF/MEK/ERK signaling pathway is Ephrin type-A receptor A2 (EPHA2)[16]. EPHA2 overexpression is common in many cancers and EPHA2 phosphorylation maintains cancer cell motility, survival and proliferation all of which promote tumor malignancy (Fig. 2)[17-19]. EPHA2 phosphorylation is induced not only by RSK but also by AKT. Therefore,

EPHA2 phosphorylation is closely related to the EGFR signaling pathway[20,21].

EGFR overexpression is observed in about 80% of CRCs, and is significantly associated with tumor stage[22]. The therapeutic effects of anti-EGFR antibodies inhibit ligand binding to the EGFR. This leads to the inhibition of EGFR phosphorylation, which blocks the subsequent activation of downstream pathways that promote cancer malignancy. Thus, the EGFR is a prime drug target for treating CRC. Anti-EGFR antibodies have been confirmed to be effective for treating CRC, but in unselected patient populations, the efficacy of anti-EGFR antibodies is generally limited to a small proportion of patients. The treatment inefficacy of the anti-EGFR antibodies in mCRC with a *RAS* mutation, where downstream signaling is activated irrespective of EGFR ligand binding, underscores that signaling inhibition is critically important for the anticancer efficacy of the anti-EGFR antibodies[23].

Even though panitumumab and cetuximab both target the EGFR, there are fundamental differences between these two anti-EGFR antibodies. For example, these two antibodies have different binding sites on the EGFR. In addition, panitumumab is a fully human monoclonal antibody compared to cetuximab, a human/mouse chimeric monoclonal antibody. With respect to toxicity, panitumumab has a reduced risk of infusion reactions (allergic reactions) compared to cetuximab due to its fully humanized nature[24,25].

The purpose of this dissertation was to characterize the pharmacological action of panitumumab by evaluating the antitumor effects and pharmacological actions after combination drug therapy or after varying the sequential order of drug treatment. These studies were conducted with a mouse model transplanted with human CRC cells. I analyzed the pharmacological action of panitumumab in combination with TAS-102 in the first chapter of this dissertation. In the second chapter of this thesis, I compared the pharmacological action of panitumumab and bevacizumab administration in this order to the same drugs administered in the opposite order.

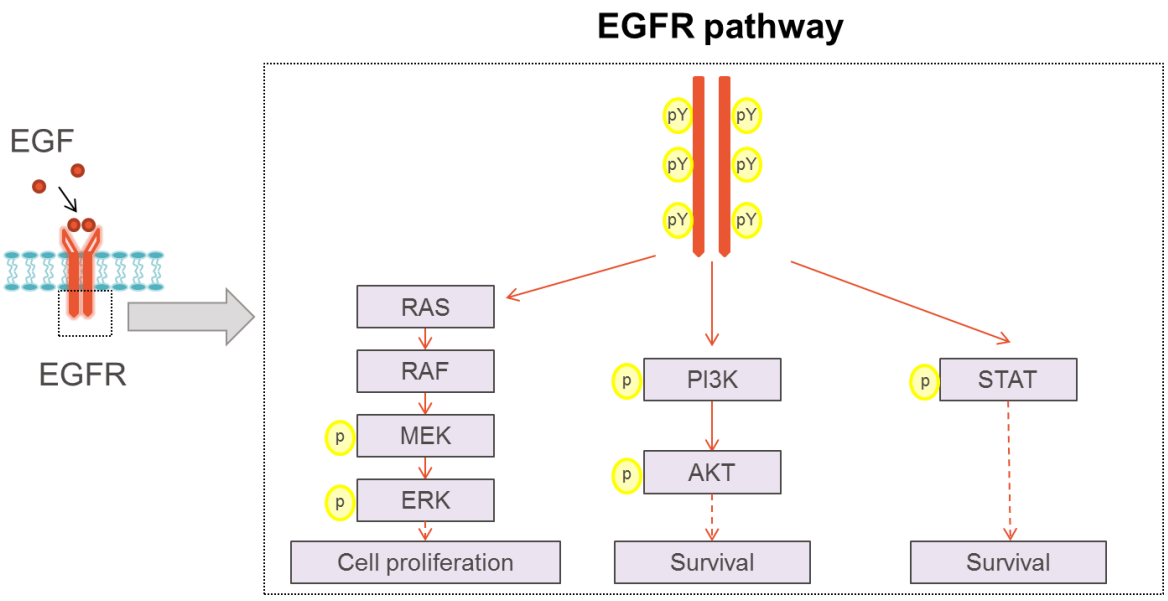

Figure 1. EGFR downstream signaling pathways. Activation of EGFR upon ligand binding leads to cell proliferation, survival and angiogenesis due to the activation of the RAS/RAF/MEK/ERK, PI3K/AKT and STAT.

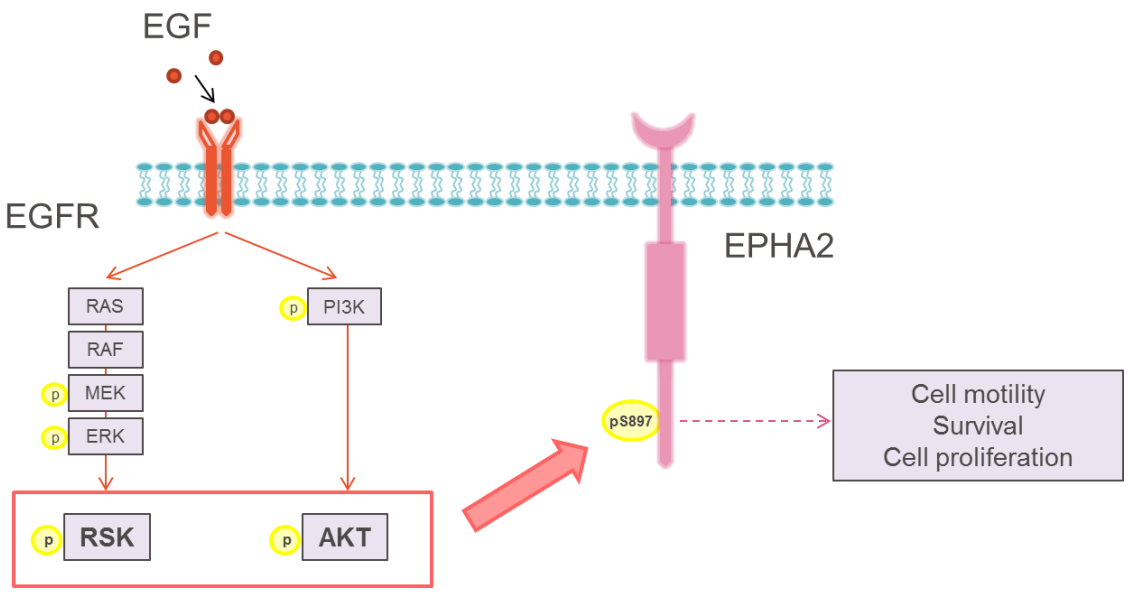

Figure 2. Function of the EPHA2 pathway.RSK and AKT induce EPHA2 (S897) phosphorylation which maintains cancer cell motility, survival and proliferation to promote tumor malignancy.

Chapter 1

Panitumumab interaction with TAS-102 leads to combinational anticancer effects via blocking of EGFR-mediated tumor response to trifluridine

Abstract

Panitumumab is a monoclonal antibody developed against the human epidermal growth factor receptor (EGFR). TAS-102 is a novel chemotherapeutic agent containing trifluridine (FTD) as the active cytotoxic component. Both panitumumab and TAS-102 have been approved for the treatment of metastatic colorectal cancer. In this study, I revealed the mechanism underlying the anticancer effects of panitumumab/TAS-102 combination using preclinical models. Panitumumab/FTD co-treatment showed additive antiproliferative effects in LIM1215 and synergistic antiproliferative effects in SW48 colon cancer cells. Consistent with the *in vitro* effects, panitumumab/TAS-102 combination caused tumor regression in LIM1215 and COL-01-JCK colon cancer patient-derived xenograft models. In LIM1215 cells, FTD induced extracellular signal-regulated kinase (ERK)/protein kinase B (AKT)/signal transducer and activator of transcription 3 (STAT3) phosphorylation and subsequent serine/threonine phosphorylation of EGFR, while it had no effects on EGFR tyrosine phosphorylation. Panitumumab and the tyrosine kinase inhibitor erlotinib reduced the basal level of EGFR tyrosine phosphorylation and reversed FTD-induced ERK/AKT/STAT3 and EGFR serine/threonine phosphorylation. These results suggested that FTD in combination with the basal activity of EGFR tyrosine kinase induced downstream prosurvival signaling through ERK/AKT/STAT3 phosphorylation. Collectively, I

propose that panitumumab interacts with FTD by targeting EGFR-mediated adaptive responses, thereby exerting anticancer effects when used in combination with TAS-102. These preclinical findings provide a compelling rationale for evaluating the combination of anti-EGFR antibodies with TAS-102 against metastatic colorectal cancer.

Introduction

Randomized trials in first-line setting combining cetuximab with FOLFILI (irinotecan/5-fluorouracil (5-FU) /leucovorin) or FOLFOX (oxaliplatin/5-fluorouracil (5-FU)/leucovorin) or panitumumab with FOLFOX demonstrated a significant survival benefit compared with that of chemotherapy alone. Although the use of cetuximab and panitumumab is restricted only to metastatic colorectal cancer (mCRC) patients with *KRAS* (Kirsten rat sarcoma viral oncogene homolog) and *NRAS* wild-type genes owing to the well-established link between *RAS* (rat sarcoma GTPase) mutations and lack of response to antibodies[26-28], these EGFR-targeting monoclonal antibodies have expanded the range of treatment options for mCRC[29].

TAS-102 is a novel, orally administered combination of a nucleoside analog trifluridine (FTD) and thymidine phosphorylase inhibitor tipiracil hydrochloride (TPI), at a molar ratio of 1:0.5[30,31]. FTD is the active cytotoxic component of TAS-102, while TPI plays a role in preventing the rapid degradation of FTD to its inactive form by thymidine phosphorylase[32]. FTD is sequentially phosphorylated; its monophosphate form (FTD-MP) transiently inhibits thymidylate synthase (TS), and its triphosphate form (FTD-TP) is incorporated into DNA[33-37] . TS inhibition is a major mechanism of action of classical fluoropyrimidines such as 5-FU[38]. Although, TS inhibition by FTD-MP may partly account for the antitumor effects of FTD[35,39], the incorporation of FTD-TP into

DNA and the resulting DNA damage appear to be the major mechanism of action of FTD[37,40,41]. Importantly, TAS-102 exhibits antitumor activity against FU-resistant cell lines in preclinical xenograft models[42-44]. Compared with the placebo, TAS-102 provided an overall survival benefit of approximately 2 months in a randomized phase III trial that included patients with refractory (or intolerant) mCRC[45].

TAS-102 is also a promising candidate for combination therapy with other agents that serve as a backbone chemotherapy, especially for the treatment of mCRC refractory to initial 5-FU-based chemotherapy. The combination of anti-EGFR antibodies and TAS-102 is effective preclinically; however, the exact mechanism underlying the combination effects remains to be elucidated[46]. In the present study, I evaluated the anticancer efficacy and molecular mechanism of a combination of panitumumab and TAS-102 in *in vitro* and *in vivo* colon cancer models.

Materials and Methods

Cells and reagents

The human colon cancer cell lines SW48 and LIM1215 were obtained from Horizon Discovery (Cambridge, UK) and DS Pharma Biomedical (Osaka, Japan), respectively. SW48 cells were cultured in McCoy's 5A medium (Wako, Osaka, Japan) with 10% fetal bovine serum (FBS). LIM1215 cells were cultured in RPMI 1640 medium (Wako) with 10% FBS, 1 μg/mL hydrocortisone (Sigma, St. Louis, MO), 0.6 μg/mL insulin (Thermo Fisher Scientific, Waltham, MA), and 10 μM 1-thioglycerol (Wako).Other human colon cancer cells, HCT-8, HCT-15, HCT-116, COLO-205 (ATCC), CW-2 (RIKEN, Saitama, Japan), and COLO-201 (JCRB, Osaka, Japan), were cultured in RPMI 1640 medium (Wako) with 10% fetal bovine serum (FBS; Thermo Scientific). WiDr and RKO cells (ATCC, Manassas, VA) were cultured in E-MEM (Wako) with 10% FBS, MEM non-essential amino acid solution (Wako), and 1 mM sodium pyruvate (Wako). HT-29 and DLD1 cells (Horizon Discovery) were cultured in McCoy's 5A medium (Wako) with 10% FBS. SW480, SW620, and SW948 cells (ATCC) were cultured in L15 medium (Thermo Scientific) with 10% FBS. COLO320DM cells (JCRB) were cultured in DMEM (Wako) with 10% FBS. Panitumumab was provided by Amgen, Inc. (Thousand Oaks, CA). Cetuximab was purchased from Merck Serono (Darmstadt, Germany). FTD was purchased from Tokyo Chemical

Industry (Tokyo, Japan). TPI was purchased from Biochempartner (Wuhan, China). Erlotinib was purchased from Selleck Chemicals LLC (Houston, TX). U0126, LY294002, and SB203520 were purchased from Wako. Trametinib was purchased from Cayman Chemical Company (Ann Arbor, MI). All antibodies used in the study were purchased from Cell Signaling Technology (Danvers, MA), except anti-glyceraldehyde 3-phosphate dehydrogenase (GAPDH) antibody (Merck Millipore, Billerica, MA).

Cell proliferation and clonogenic assay

For the cell proliferation assay, colon cancer cells were plated in 96-well plates at appropriate densities. Serial dilutions of FTD, panitumumab, and FTD/panitumumab as well as dimethyl sulfoxide (DMSO; control) were added to the culture media 24 h after cell plating. The cells were then cultured for an additional 72 h, and cell viability was determined by the CellTiter-Glo assay (Promega, Fitchburg, WI).

For the clonogenic assay, 1×10^3 SW48 or LIM1215 cells were plated in each well of 6-well plates and subsequently treated with FTD, panitumumab, FTD/panitumumab in combination, or DMSO for 14 days. The cell colonies were stained with 0.5% crystal violet and counted using a GelCount colony counter (Oxford Optronix, Abingdon, UK)[47].

Analysis of drug combination effects

Calculation of the combination metrics was performed as described previously[48]. Briefly, isobologram analysis was used to determine the effects of drug combinations. A nine-parameter response surface model was used to fit the relationship between normalized viability and drug concentrations[49]. To quantify the combined effects of two drugs, a combination index (CI)[50,51] or nonlinear blending[52] was computed. A CI value below 0.7 was classified as synergy, while a value above 1.3 was classified as antagonism. A value in the range between 0.7 and 1.3 was considered to be additive. Nonlinear blending was applied to determine synergy if the maximum inhibition by a single agent was less than 50%. A blending value above 20 was classified as synergy, while that below −20 was classified as antagonism.

Western blotting

LIM1215 cells were plated at a density of 5×10^5 cells/well in 6-well plates. One day later, the cells were treated with FTD, panitumumab, erlotinib, U0126, LY294002, SB203520, or DMSO for 24 h. The cells were then washed once with cold phosphate-buffered saline and lysed in lysis buffer (62.5 mM Tris–HCl [pH 7.5], 10% glycerol, 1% sodium dodecyl sulfate [SDS]) supplemented with protease inhibitor cocktail set II and phosphatase inhibitor cocktail set III (Merck Millipore). After centrifugation, the protein concentrations of the cell lysates were determined using the bicinchoninic acid (BCA) protein assay reagent (Thermo Fisher Scientific). The cell lysates were

mixed with Laemmli SDS sample buffer, heated, and subjected to SDS/PAGE, followed by immunoblotting. Detection was performed using an enhanced chemiluminescence reagent (GE Healthcare, Chicago, IL, USA).

Stable isotope labeling with amino acids in a cell culture-based phosphoproteomics analysis

LIM1215 cells were cultured in stable isotope labeling with amino acids in cell culture (SILAC) K8R10 medium for heavy samples or K0R0 medium for light samples (Thermo Scientific), supplemented with 10% dialyzed FBS (Thermo Scientific), 100 mg/L L-proline (Sigma), 1 μg/mL hydrocortisone (Sigma), 0.6 μg/mL insulin (Thermo Fisher Scientific), and 10 μM 1-thioglycerol (Wako). After treatment with FTD alone, panitumumab alone, FTD/panitumumab combination, or DMSO for 24 h, the cells were lysed in ice-cold lysis buffer (20 mM Tris–HCl [pH 7.4], 0.1% SDS, 1% NP-40, 1 mM ethylenediaminetetraacetic acid, protease inhibitor cocktail (Sigma), and phosphatase inhibitors cocktail (Sigma)). Equal amounts of protein from light and heavy samples were mixed, and the proteins were precipitated with five volumes of acetone. The precipitates were dissolved in 8 M urea, 100 mM triethylammonium bicarbonate (TEAB; Wako), and 5 mM tris(2-carboxyethyl)phosphine (Thermo Scientific). The samples were digested with Lys-C protease (Wako) at a ratio of 1:200 for 4 h, after which 50 mM iodoacetamide (Wako) was added for alkylation. The samples were diluted with 20 mM TEAB to 1 M urea

concentration and then digested with sequencing-grade modified trypsin (Promega) at a ratio of 1:100. The digested samples were acidified with 0.5% trifluoroacetic acid, and the supernatants were subsequently desalted on a C18 column (Shiseido C18MG, 4.6 × 250 mm, Tokyo, Japan). The desalted peptides were loaded onto TiO_2 chips (GL Science, Tokyo, Japan) to enrich phosphopeptides in accordance with the instruction manual. The eluted phosphopeptides were desalted on a C18 column (Shiseido C18MG, 2.0 × 10 mm). The phosphopeptides were separated into 16 fractions on a polysulfoethyl A SCX column (PolyLC, 2.1 × 35 mm, 5 μm, 300 Å) using a gradient changing from buffer A (0.1% formic acid and 80% acetonitrile [MeCN]) to buffer B (350 mM ammonium formate, 30% MeCN, pH 3). The fractionated peptides were analyzed using fusion mass spectrometry (MS) (Thermo Scientific) coupled to a nano-liquid chromatography (LC) system (EASY-nLC 1000). The peptides were loaded onto a trap column (C18 Pepmap100, 3 μm, 0.075 × 20 mm) and separated on an analytical column (Reprosil-Pur C18AQ, 3 μm, 0.075 × 150 mm; Nikkyo Technos, Tokyo, Japan) at a flow rate of 300 nL/min for 90 min. LC/MS/MS measurements were performed by acquiring MS spectra at a resolution of 120,000 at 200 m/z, and data-dependent higher-energy collisional dissociation MS/MS at 30% normalized collision energy of the 30 most abundant ions in the ion trap. The dynamic exclusion time was 12 s. All MS raw files were processed to identify and quantify peptides with Proteome Discoverer 1.4 (Thermo Scientific)

using Mascot (v. 2.5, Matrix Science, London, UK) against the UniProt human protein database. The mass tolerances of a precursor and fragment were set to 10 ppm and 0.3 Da, respectively. A false discovery rate of 0.01 was applied to peptide identification.

Subcutaneous tumor xenograft models

All in vivo procedures were conducted in compliance with the Guide for the Care and Use of Laboratory Animals (8th Edition), US National Research Council, and approved by the Institutional Animal Care and Use Committee of the Shonan Research Center (#00011823), Takeda Pharmaceutical Company, Ltd. Female BALB/cA Jcl-nu/nu (nude) mice and C.B17/Icr-scid/scid Jcl (SCID) mice (CLEA, Tokyo, Japan) were maintained under specific pathogen-free conditions. LIM1215 cells (5×10^6) mixed with Matrigel were inoculated subcutaneously into the right flank of six- to seven-week-old SCID mice. Once established, the tumors were surgically excised, and smaller tumor fragments (about 2 mm in diameter) were subcutaneously implanted in the right flank of SCID mice. To establish the patient-derived colon tumor xenograft (PDX) model, COL-01-JCK PDX line was obtained from the Central Institute for Experimental Animals (Kawasaki, Japan), and tumor fragments were implanted into the right flank of female nude mice. The mice were randomized when the mean tumor volume reached approximately 50–200 mm^3. The mice were then treated with the vehicle (0.5% hydroxypropyl methylcellulose solution or saline),

panitumumab (intraperitoneally), TAS-102 (a mixture of FTD and TPI at a molar ratio of 1:0.5 (orally)), or panitumumab/TAS-102 combination for 2 weeks. The tumor volumes were measured twice weekly with Vernier calipers, and calculated as the length × width^2 × 0.5. The treated/control ratio (T/C, %) was calculated by dividing the change in tumor volume in the drug-treated mice by that in the vehicle-treated control mice. The percentage of tumor regression was calculated as follows: Tumor regression (%) at day X = [1-(tumor volume at day X/tumor volume at day 0)] × 100. Statistical comparisons of tumor volumes and body weights were performed using Dunnett's multiple comparison tests; $p < 0.05$ was considered statistically significant.

Immunohistochemical staining of paraffin-embedded samples

Tumor-bearing mice, subcutaneously injected with LIM1215 cells, were administered the vehicle, TAS-102 (75 mg/mL, twice daily from day 1 to day 4), panitumumab (3 mg/mL, on days 1 and 4), or TAS-102/panitumumab. Tumor xenografts were excised on day 5, fixed with 10% neutral buffered formalin for 24 h, and embedded in paraffin. Sliced sections were deparaffinized with xylene, then rehydrated, and subjected to citrate buffer antigen retrieval (98°C, 40 min). Immunohistochemical staining for FTD was performed as described previously [53] using an anti-BrdU antibody (clone 3D4; BD Pharmingen, Franklin Lakes, NJ) and a peroxidase-conjugated anti-mouse antibody (Histofine Simplestain Max PO, Nichirei, Tokyo, Japan). Peroxidase activity

was detected with diaminobenzidine. Sections were counterstained with hematoxylin, and stained images were acquired with a Nanozoomer digital slide scanner (Hamamatsu Photonics, Shizuoka, Japan). FTD-positive nuclei were automatically counted by setting a fixed threshold to remove the background, and the percentage of FTD-positive nuclei relative to all nuclei was determined with the image analysis software Tissue Studio (Definiens, Munich, Germany).

Network analysis

The NetworKIN (version 3.0) algorithm was used for the prediction of potential kinase–substrate relationships[54]. The NetworKIN algorithm combines network-proximity scores for protein–protein interactions and NetPhorest probabilities on the basis of network distances and peptide sequences, respectively. Phosphopeptides with fold changes of at least 1.5 in duplicate samples after treatment with FTD alone were selected as altered phosphopeptides. For network analysis, the kinase–substrate relationships of the altered phosphopeptides were filtered to include only those with a NetworKIN score of >2, and kinases that altered phosphopeptides were selected. Cytoscape (version 3.4.0) was used for network data integration, analysis, and visualization for the selected kinases and substrates[55].

Pathway enrichment analysis

Kyoto Encyclopedia of Genes and Genomes (KEGG) enriched pathways were analyzed using

the Database for Annotation, Visualization, and Integrated Discovery (DAVID) Bioinformatics Resources 6.8[56,57]. Phosphopeptides with a fold change of at least 2 in duplicate samples after treatment with each drug were selected as a list of altered phosphopeptides. Phosphopeptides detected in duplicate samples were used as a background list. Enrichment p values of < 0.05 were considered significant.

Results

The combination of panitumumab and FTD has significant antiproliferative effects in colon cancer cells

First, I evaluated the in vitro antiproliferative effects of panitumumab and FTD combination in SW48 and LIM1215 cells, which harbor the wild-type *KRAS* and *BRAF* genes (Fig. 3A and B). Panitumumab blocked SW48 and LIM1215 cell proliferation in a dose-dependent manner, although the maximum inhibition rates remained around 40 and 60%, respectively. FTD significantly inhibited proliferation of SW48 and LIM1215 cells with IC_{50} values of 8.1 and 0.57 μM, respectively. Co-treatment with FTD and panitumumab produced synergistic combination effects in SW48 cells (non-linear blending score >20) and additive combination effects in LIM1215 cells (0.7<CI<1.3). Combination effects were also seen between FTD and cetuximab, another anti-EGFR antibody, in LIM1215 cells but not in WiDr cells harboring the *BRAF* V600E mutation (Fig. 4). In clonogenic assays, co-treatment with panitumumab/FTD significantly suppressed colony formation and growth of SW48 and LIM1215 cells (Fig. 5). Quantification analysis revealed that SW48 cell colony areas decreased by 75% when treated with 3 μM FTD and 50 ng/mL panitumumab, while those of LIM1215 decreased by 87% at even lower concentrations, that is, 0.3 μM FTD and 5 ng/mL panitumumab. FTD showed a broad spectrum of anticancer activities

against various colon cancer cell lines, irrespective of *KRAS* or *BRAF* mutation status, with IC_{50} values ranging from single to low double-digit micromolar concentrations (Fig. 6). LIM1215 cells were highly sensitive to FTD compared to other colon cancer cells (Fig. 3B). Therefore, LIM1215 cells were used to investigate the interaction between panitumumab and FTD further.

The combination of panitumumab/FTD leads to tumor regression in subcutaneous colon cancer xenograft models

Colon cancer xenograft mouse models were used to evaluate the combination effects of panitumumab/TAS-102 in vivo. SCID mice were inoculated subcutaneously with LIM1215 cells. After the tumors reached appropriate volumes, the mice received panitumumab (3 mg/kg, twice weekly; intraperitoneally), TAS-102 (75 mg/kg, twice daily on a 5-days-on/2-days-off schedule; orally), their combination, or the vehicle for 2 weeks. As shown in Fig. 7A, treatment with panitumumab alone and TAS-102 alone resulted in statistically significant tumor growth suppression with T/C values of 3.8 and 17.9%, respectively, on day 14 ($p < 0.001$). The combination treatment had more profound antitumor effects, leading to substantial tumor regression, with a maximum regression rate of 63.2% on day 18. In this model, the mean body weight of the vehicle-treated mice decreased gradually over the experimental period (Fig. 7C). However, 2-week treatments with panitumumab, TAS-102, or the combination were tolerated and

caused less body weight loss than vehicle treatment on day 21. To extend these findings, I conducted a similar efficacy study using a COL-01-JCK PDX model. COL-01-JCK is a colon PDX line without *KRAS* and *BRAF* mutations. TAS-102 moderately inhibited tumor growth in this model, with the lowest T/C value of 33.4% on day 14 ($p < 0.01$; Fig. 7B). In contrast, panitumumab treatment led to significant regression of tumor xenografts during the treatment period (by 36.1% on day 18 vs. day 0). Combination of panitumumab and TAS-102 resulted in greater tumor regression than panitumumab alone, and the regression continued for more than 3 weeks after drug withdrawal (by 68.7% on day 35 vs. day 0). Although body weight loss was observed in the vehicle-treated mice in this PDX model as well, all drug treatments were generally tolerated (Fig. 7D).

In addition, the effect of panitumumab on FTD incorporation into DNA was examined with an anti-5-bromo-2-deoxyuridine (BrdU) antibody because FTD incorporated into DNA can be recognized by BrdU antibodies[53]. Immunohistochemical staining experiments showed that there was no statistically significant difference in the percentage of FTD-positive nuclei in tumor xenografts between the mice treated with FTD alone and those treated with FTD/panitumumab combination (Fig. 8).

Panitumumab blocks FTD-induced ERK and AKT activation as well as EGFR gel mobility

shift

To determine the potential interaction between panitumumab and FTD in EGFR signaling, I analyzed the phosphorylation status of signaling mediators ERK and AKT in FTD-treated colon cancer cells using western blotting. Consistent with the results of a previous study[58], ERK1/2, AKT, and STAT3 phosphorylation was induced in SW48 and LIM1215 cells after exposure to 3 μM FTD for 16 h or longer (Fig. 9). I tested whether panitumumab affected FTD-induced phosphorylation of ERK1/2 and AKT and observed that co-treatment of panitumumab with FTD for 24 h suppressed FTD-induced AKT and ERK phosphorylation (Fig. 10). Notably, FTD treatment also led to a slight EGFR gel mobility shift, suggesting that it modified EGFR to a certain extent. However, this EGFR mobility shift was inhibited by co-treatment with panitumumab.

FTD induces serine/threonine but not tyrosine phosphorylation of EGFR

I performed SILAC-based phosphoproteomics analysis to investigate FTD-induced EGFR modification and cellular signaling activation further. The results of pathway analyses based on proteomic data confirmed the pharmacodynamic effects of FTD and panitumumab in LIM1215 cells. FTD treatment led to the significant enrichment of several Kyoto Encyclopedia of Genes and Genomes pathways associated with DNA damage, such as the Fanconi anemia pathway, cell cycle, homologous recombination, and p53 signaling (Table 1). Panitumumab treatment decreased the

phosphopeptides derived from MAPK1 (ERK2), MAPK3 (ERK1), and ribosomal protein S6 kinases A1 and A3, suggestive of EGFR signaling inhibition by panitumumab (Tables 2 and 3).

As FTD-induced gel mobility shift of EGFR occurred in parallel with AKT and ERK phosphorylation and was reversed by co-treatment with panitumumab, I speculated that FTD might have induced EGFR tyrosine phosphorylation. However, SILAC-based analyses revealed that FTD-induced EGFR phosphorylation occurred at serine/threonine residues rather than at tyrosine residues (Table 2). Consistently, western blotting confirmed that FTD stimulated EGFR phosphorylation at threonine (T) 669 and serine (S) 1046/1047, but not at known tyrosine phosphorylation sites (Fig. 11A). The time dependence and concentration dependence of FTD-induced EGFR serine/threonine phosphorylation were confirmed in additional experiments (Figs. 12 and 13). Panitumumab alone reduced the basal levels of EGFR tyrosine phosphorylation at almost all sites tested (Fig. 11A). Moreover, co-treatment with panitumumab suppressed FTD-induced serine/threonine phosphorylation of EGFR. Increase in TS protein level, a pharmacodynamic marker of inhibition of TS activity by fluoropyrimidine derivatives [59], was observed with a similar extent in cells treated with both FTD alone and FTD/panitumumab combination. These results suggest that co-treatment with panitumumab has little effects of FTD on TS inhibition, although TS inhibition is not considered to be the main mechanism underlying FTD

cytotoxicity.

Serine/threonine phosphorylation of EGFR is dependent on the activation of MEK–ERK signaling pathway

To investigate the mechanism underlying FTD-induced serine/threonine phosphorylation of EGFR, LIM1215 cells were co-treated with FTD and several kinase inhibitors (Fig. 11B). FTD-induced EGFR serine/threonine phosphorylation was suppressed by erlotinib and panitumumab. It was also blocked by the MEK inhibitor U0126. The PI3K inhibitor LY294002 inhibited FTD-induced AKT/STAT3 phosphorylation, but not FTD-induced ERK1/2 and EGFR serine/threonine phosphorylation. In addition, the time dependence and concentration dependence between FTD-induced ERK1/2 phosphorylation and EGFR serine/threonine phosphorylation (Figs. 12 and 13) were similar. Using the SILAC-based phosphoproteomic data, I determined the responsible kinases and their substrates that were affected by FTD treatment and created a kinase–substrate connected network (Fig. 14). A subnetwork of EGFR and the first neighbors showed significant contributions of ERK1/2 (MAPK3 and MAPK1, respectively) to FTD-induced serine/threonine phosphorylation of EGFR. These results suggest that EGFR serine/threonine phosphorylation occurs downstream of MEK–ERK signaling pathway.

FTD also induced p38 MAPK phosphorylation (Fig. 11B, Table 1), which was not affected by

either panitumumab or erlotinib, suggesting that upstream signaling through p38 MAPK phosphorylation and ERK/AKT/STAT3 phosphorylation was differentially induced by FTD. However, FTD-induced AKT/STAT3 and EGFR S1046/1047 phosphorylation was inhibited by the p38 MAPK inhibitor SB203580, suggestive of signaling crosstalk.

Co-treatment with a MEK inhibitor and FTD shows additive antiproliferative effects

As the MEK inhibitor U0126 blocked FTD-induced AKT/ERK/STAT3, EGFR T669, and S1046/1047 phosphorylation to a similar extent as panitumumab, the effect of co-treatment with FTD and the MEK inhibitors U0126 or trametinib on cell proliferation was evaluated. Co-treatment with either FTD/U0126 or FTD/trametinib yielded additive antiproliferative effects in LIM1215 cells ($0.7<CI< 1.3$; Fig. 15).

Discussion

In this study, I demonstrated that the combination treatment of TAS-102 and panitumumab exerted significant anticancer activity compared to that achieved by single-agent treatment in *in vitro* and *in vivo* wild-type *KRAS* colon cancer models. Previous studies suggested that TAS-102 may potentially enhance the effects of combination treatment of chemotherapeutics irinotecan and oxaliplatin[60,61] or targeted therapeutics, such as bevacizumab and anti-EGFR agents[46,58]. My results are consistent with that of Tsukihara et al.[46], wherein TAS-102/panitumumab combination suppresses tumor growth in an SW48 tumor xenograft model. However, the *in vivo* combination efficacy was prominent in LIM1215 and COL-01-JCK models used in this study when compared with that in SW48 model, as reflected by the profound and sustained tumor regression achieved with a similar dosing regimen. The difference in responses among these wild-type *KRAS* colon cancer models may provide an intriguing tool for exploring determinants or predictive markers of the response. In my two models, the vehicle-treated mice experienced gradual body weight loss as the tumors grew, which was probably due to cancer-related cachexia. However, the combination regimen was tolerated and had no confounding effects on body weight loss caused by TAS-102, suggesting that TAS-102 and panitumumab had few overlapping toxicities. Indeed, the most frequently observed adverse events associated with TAS-102 in a phase III study were neutropenia

and leukopenia[45], while those associated with panitumumab were skin toxicities, hypomagnesemia, and diarrhea[5]. However, panitumumab has no cross-reactivity with mouse EGFR, which makes it difficult to assess the therapeutic window in tumor xenograft models. Thus, careful evaluation of safety is needed in clinical settings.

I also assessed the molecular mechanism underlying the interaction between FTD and panitumumab, and found that FTD treatment induced ERK1/2, AKT, and STAT3 phosphorylation in SW48 and LIM1215 cells. Several other chemotherapeutics induced similar ERK/AKT/STAT3 activation, which is considered to mediate prosurvival signaling and be implicated in resistance to these genotoxic agents[62-67]. Thus, I believe that FTD-induced activation of ERK/AKT/STAT3 plays a similar role in the adaptive response of colon cancer cells to genotoxic stress caused by FTD. In particular, the MEK inhibitors U0126 and trametinib when combined with FTD caused additive effects on the proliferation of LIM1215 cells. Therefore, I believe that MEK–ERK signaling may, at least partly, mediate prosurvival signaling in response to FTD.

I further observed that FTD-induced ERK/AKT/STAT3 phosphorylation was suppressed by panitumumab and erlotinib. Initially, these results led us to speculate that FTD could induce EGFR tyrosine kinase activation and subsequent phosphorylation of its downstream molecules. However, SILAC-based proteomics and western blotting revealed that FTD had no effects on EGFR tyrosine

phosphorylation status. Instead, FTD induced EGFR serine/threonine phosphorylation, which was reversed by combination treatment with panitumumab, erlotinib, or the MEK inhibitor U0126. Therefore, I proposed a model in which the basal activity of EGFR tyrosine kinase is required for FTD-induced ERK/AKT/STAT3 phosphorylation, and in which EGFR serine/threonine phosphorylation is a downstream event of MEK–ERK signaling. This model is also supported by kinase–substrate connected network analysis based on phosphoproteomics data, which indicate an important contribution of ERK1/2 to FTD-induced EGFR serine/threonine phosphorylation. Consistent with these data, prior studies have implicated threonine 669 of EGFR as an ERK phosphorylation site[68-70].

The significance of FTD-induced EGFR serine/threonine phosphorylation, however, remains to be elucidated. Nishimura et al.[71] showed that tumor necrosis factor alpha- (TNF-α) induced EGFR phosphorylation at T669 and S1046/1047 stimulated EGFR endocytosis, leading to the survival of cells exposed to TNF-α receptor death signal. Further, Winograd-Katz and Levitzki[64] proposed that cisplatin-induced EGFR T669 phosphorylation similarly increased EGFR endocytosis, which might switch signaling pathways from proliferation to survival. Thus, it is of interest to further investigate whether FTD-induced EGFR serine/threonine phosphorylation mediates similar prosurvival signaling through EGFR endocytosis in colon cancer cells. One

possible approach is to introduce mutations that prevent phosphorylation by substitution of serine/threonine residues of EGFR and evaluate FTD sensitivity of the cells with these mutant EGFRs.

I also observed that FTD treatment induced phosphorylation of p38 MAPK. p38 MAPK phosphorylation is induced by a diverse set of intra- and extracellular stimuli, including genotoxic stress caused by chemotherapeutics such as cisplatin mediating prosurvival signaling[64]. Unlike ERK/AKT/STAT3 phosphorylation, FTD-induced p38 MAPK phosphorylation was not significantly affected by panitumumab or erlotinib, suggesting that p38 MAPK phosphorylation was independent of EGFR tyrosine kinase activity. However, pharmacological inhibition of p38 MAPK decreased FTD-induced AKT, STAT3, and EGFR S1046/1047 phosphorylation. These results suggest that there is a crosstalk between p38 MAPK and EGFR/AKT/STAT3 signaling. Accordingly, I proposed a model in which FTD-induced p38 MAPK activation and EGFR-dependent ERK/AKT/STAT3 activation cooperatively promote prosurvival signaling (Fig. 16).

In conclusion, I demonstrated that co-treatment with panitumumab and TAS-102 had significant *in vitro* and *in vivo* anticancer effects in different colon cancer models. I also showed that panitumumab suppressed FTD-induced ERK/AKT/STAT3 activation, which I believe is the

mechanism underlying the combinatorial effects of panitumumab and FTD.

Tables and Figures

Table 1. List of genes from the KEGG pathways identified by phosphoproteomic analysis, showing the effects of FTD versus control in LIM1215 cells.

KEGG Pathway	*p* value	Gene Symbol	
		Upregulated	Downregulated
Fanconi anemia pathway	0.000	*ATR ATRIP BLM BRCA1 BRCA2 BRIP1 FAN1 FANCI PALB2 POLH RPA2 USP1*	*FANCD2 FANCI RPA1*
RNA transport	0.001	*ACIN1 ALYREF EIF4G1 NCBP1 NUP153 NUP188 NUP214 NUP35 PNN POM121 POM121C POP1 POP4 RANBP2 RGPD3 RGPD4 RGPD8 RPP30 TPR XPO5*	*EIF3B NUP107 NUP133 NUP153 NUP210 NUP35 NUP50 PABPC1 PABPC1L PABPC3 PABPC4 POM121 POM121C RANBP2 RANGAP1 RGPD1 RGPD2 RGPD3 RGPD4 RGPD8 SRRM1 TPR XPO1*
Ribosome biogenesis in eukaryotes	0.006	*BMS1 MDN1 NOL6 NOP58 POP1 POP4 RBM28 RPP30 UTP14A*	*DKC1 GNL3 NOP56 TCOF1 WDR75 XPO1*
MicroRNAs in cancer	0.014	*BRCA1 CCNE1 CD44 CDCA5 EGFR ERBB2 MDM2 MET SHC1 SIRT1 SOS1 TP53*	*ABCC1 CDKN1B ERBB2 HNRNPK MAPK7 MARCKS MYC PAK4 PDCD4*
Cell cycle	0.018	*ATR BUB1B CCNE1 CDC27 CDK1 CHEK1 CHEK2 ESPL1 MCM3 MCM6 MDM2 PRKDC SMC1A SMC3 TP53*	*ANAPC2 BUB1 CDC20 CDKN1B GSK3B MCM6 MYC SMAD2 TTK*
Homologous recombination	0.021	*BLM BRCA2 NBN RAD50 RPA2*	*RPA1*
p53 signaling pathway	0.022	*ATR CCNE1 CDK1 CHEK1 CHEK2 DDB2 GTSE1 MDM2 STEAP3 TP53*	*GTSE1*
Focal adhesion	0.047	*ARHGAP35 ARHGAP5 BAD EGFR ELK1 ERBB2 FLNA JUN MET PXN SHC1 SOS1 TLN1 ZYX*	*ARHGAP5 ERBB2 FLNA FLNB GSK3B ITGB4 PAK1 PAK2 PAK4 ZYX*

Table 2. Effects of FTD on EGFR-, ERK1/2-, and p38 MAPK-derived phosphopeptides.

Name	Gene Symbol	Phosphosite	Log_2FC FTD/ctr	Log_2FC Pmab/ctr	Log_2FC (FTD + Pmab)/ctr	Sequence	Start	End
EGFR	*EGFR*	pT669	1.34	−1.02	−0.35	ELVEPL[pT]PSGEAPNQALLR	663	681
		pS967	1.07	−0.86	0.32	MHLP[pS]PTDSNFYR	963	975
		pS1002	0.02	−0.31	0.20	ALMDEEDMDDVVDADEYLIPQQGFFS[pS]PSTSR	976	1007
		pS1004	0.05	−0.29	−0.08	ALMDEEDMDDVVDADEYLIPQQGFFSSP[pS]TSR	976	1007
		pS1015	1.06	0.07	1.15	TPLLSSL[pS]ATSNNSTVACIDR	1008	1028
		pS1018	1.07	−0.05	0.74	TPLLSSLSAT[pS]NNSTVACIDR	1008	1028
		pS1039 pS1021	0.78	0.17	1.14	TPLLSSLSAT[pS]NN[pS]TVACIDR	1008	1028
		pT1017 pS1018	1.46	0.21	1.40	TPLLSSLSA[pT][pS]NNSTVACIDR	1008	1028
		pS1040	−0.70	−0.74	−0.95	NGLQSCPIKED[pS]FLQR	1029	1044
		pS1047 pT1050	2.18	0.19	1.01	YS[pS]DP[pT]GALTEDSIDDTFLPVPEYINQSVPK	1045	1075
		pS1057	0.77	−0.58	0.01	YSSDPTGALTED[pS]IDDTFLPVPEYINQSVPK	1045	1075
		pY1068	−0.15	0.16	−0.13	YSSDPTGALTEDSIDDTFLPVPE[pY]INQSVPK	1045	1075
		pS1142	0.53	−0.78	−0.45	GSHQI[pS]LDNPDYQQDFFPK	1137	1155
		pY1148	−0.09	0.09	−0.28	GSHQISLDNPD[pY]QQDFFPK	1137	1155
		pY1173	−0.08	0.01	−0.30	GSTAENAE[pY]LR	1165	1175
ERK1	*MAPK3*	pT202 pY204	0.77	−1.74	−1.91	IADPEHDHTGFL[pT]E[pY]VATR	190	208
		pY204	0.59	−0.78	−0.89	IADPEHDHTGFLTE[pY]VATR	190	208
ERK2	*MAPK1*	pT185 pY187	0.75	−2.08	−1.96	VADPDHDHTGFL[pT]E[pY]VATR	173	191
		pY187	0.55	−0.83	−1.07	VADPDHDHTGFLTE[pY]VATR	173	191
p38 alpha	*MAPK14*	pT180	0.69	0.41	1.19	HTDDEM[pT]GYVATR	174	186
		pT180 pY182	0.56	0.75	1.51	HTDDEM[pT]G[pY]VATR	174	186
		pY182	0.82	0.35	0.70	HTDDEMTG[pY]VATR	174	186
p38 delta	*MAPK13*	pT180	1.04		0.76	HADAEM[pT]GYVVTR	174	186
		pY182	0.86	0.40	1.04	HADAEMTG[pY]VVTR	174	186

Phosphopeptides derived from EGFR, ERK1/2, and p38 MAPK were identified by phosphoproteomics analysis in LIM1215 cells treated with DMSO (ctr), FTD, panitumumab (Pmab), or a combination of FTD/panitumumab (FTD + Pmab). Amino acid numbers correspond to those in the UniProt protein database, except those for EGFR, which is a mature form, with the first 24 amino acids of the signal peptide cleaved off. Log_2FC, Log_2 fold change.

Table 3. List of genes from the KEGG pathways identified by phosphoproteomic analysis, showing the effects of panitumumab versus control in LIM1215 cells.

KEGG Pathway	*p* value	Gene Symbol	
		Upregulated	Downregulated
Progesterone-mediated oocyte maturation	0.000		*ADCY3 BUB1 CDC25B HSP90AB1 MAPK1 MAPK3 RPS6KA1 RPS6KA3*
Estrogen signaling pathway	0.002	*CREB3L1*	*ADCY3 EGFR HSP90AB1 MAPK1 MAPK3 SHC1*
Oocyte meiosis	0.026		*ADCY3 BUB1 MAPK1 MAPK3 RPS6KA1 RPS6KA3*
Bladder cancer	0.036	*DAPK1*	*EGFR MAPK1 MAPK3*
Adrenergic signaling in cardiomyocytes	0.046	*CREB3L1*	*ADCY3 MAPK1 MAPK3 SLC9A1*

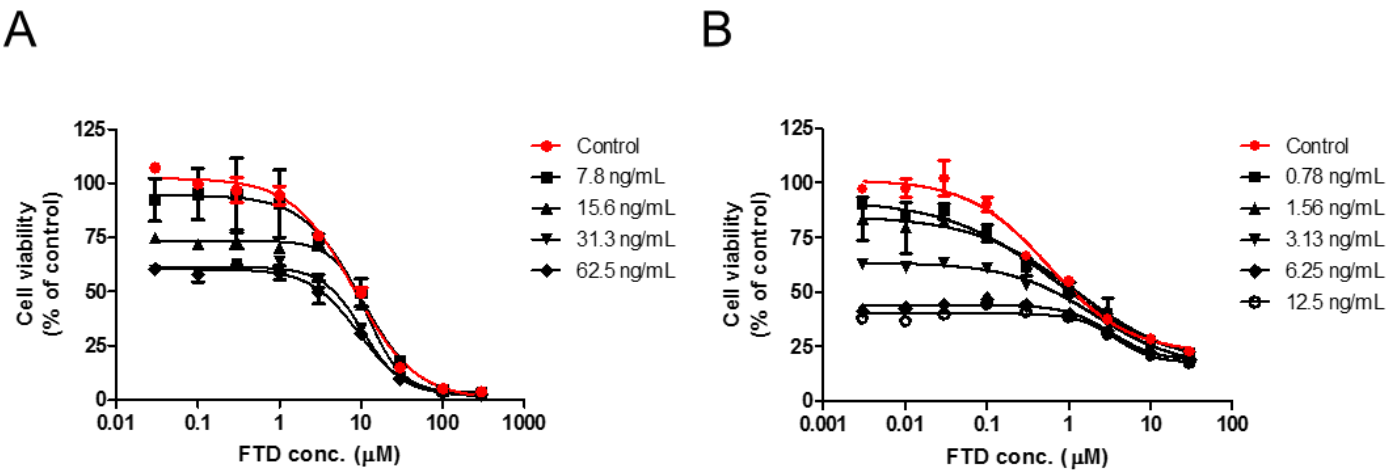

Figure 3. Panitumumab interacts with FTD to inhibit the growth of colon cancer cells. Viability of SW48 (A) and LIM1215 (B) cells after co-treatment with panitumumab and FTD for 72 h. Error bars, standard deviation.

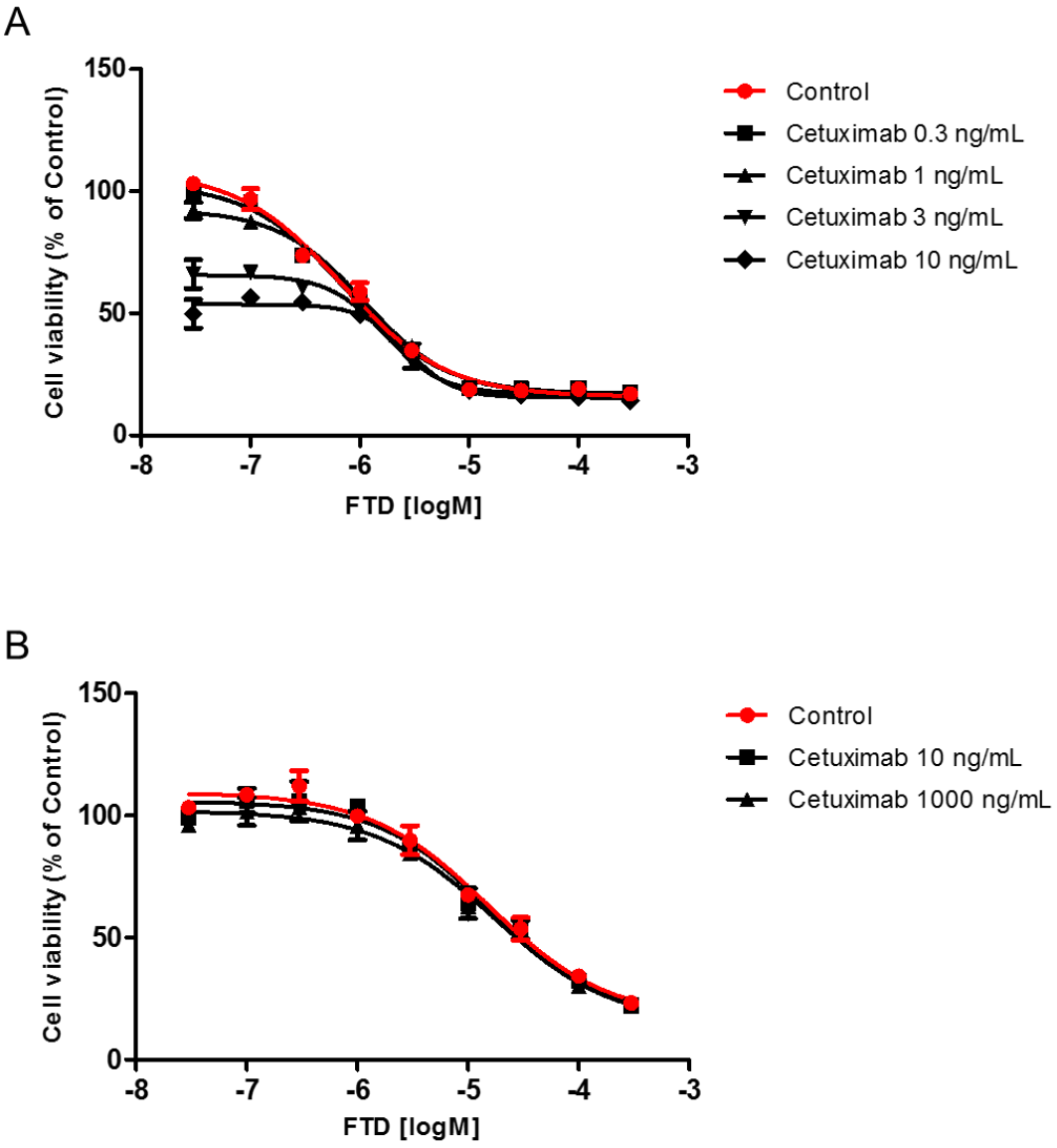

Figure 4. Co-treatment with cetuximab and FTD inhibits proliferation of LIM1215 cells but not WiDr cells. Viability of LIM1215 (A) and WiDr (B) cells after co-treatment with cetuximab and FTD for 72 h. Values represent the mean cell viability (% of control). Error bars, standard deviation.

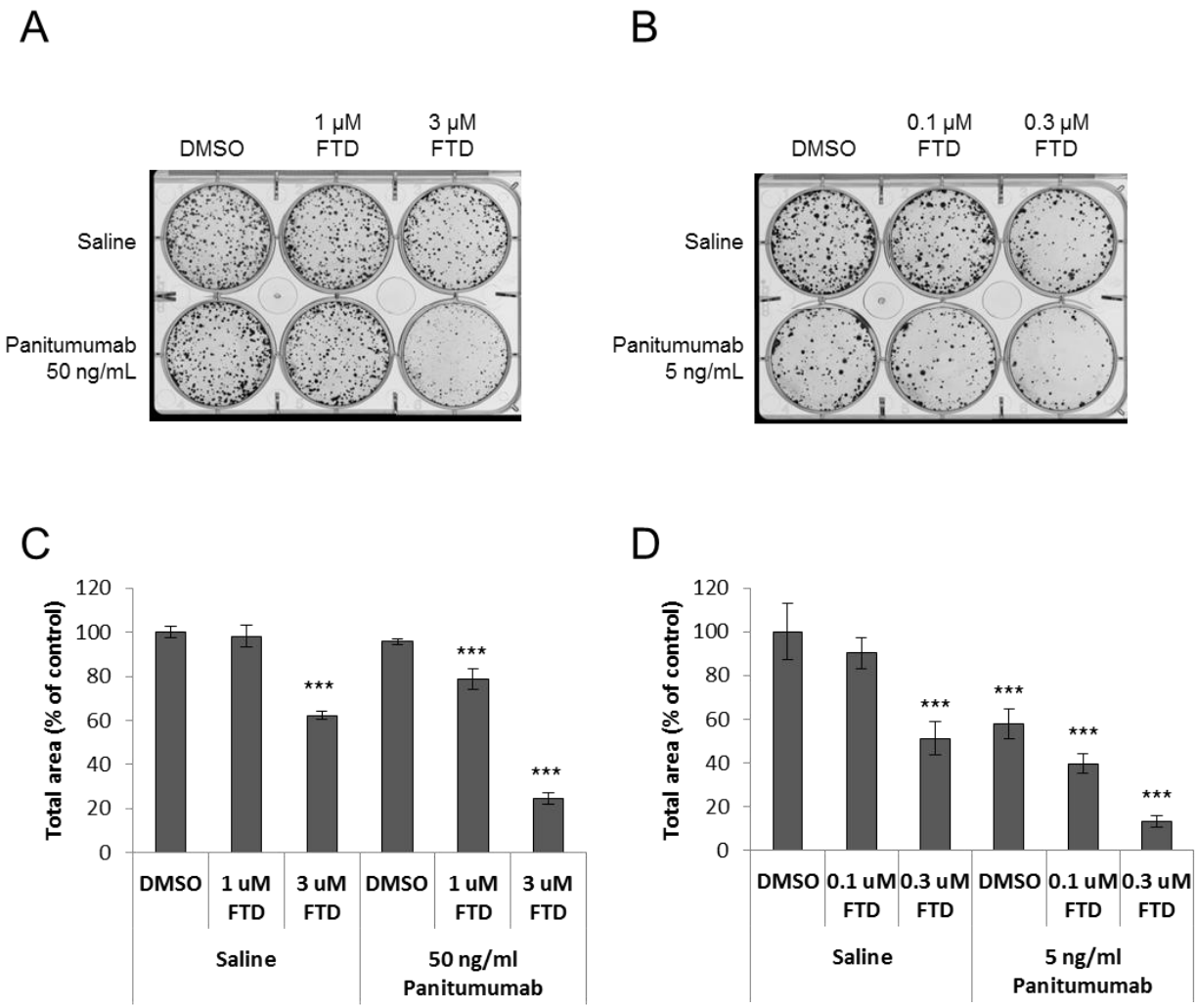

Figure 5. Panitumumab interacts with FTD to inhibit the clonogenic growth of colon cancer cells. Clonogenic survival of SW48 (A) and LIM1215 (B) cells treated with the vehicle, panitumumab alone, FTD alone, or panitumumab/FTD combination for 14 days. Representative images of colonies under different treatment are shown. Clonogenic assay were performed in triplicate for SW48 (C) and LIM1215 (D) cells. Total colony areas were individually determined using image analysis. Values represent the mean colony area (% of control). Error bars, standard deviation. Statistical comparisons of colony area were performed using Dunnett's multiple comparison tests. Asterisks denote $P < 0.001$ (***) versus the value for control colony area treated with DMSO and saline.

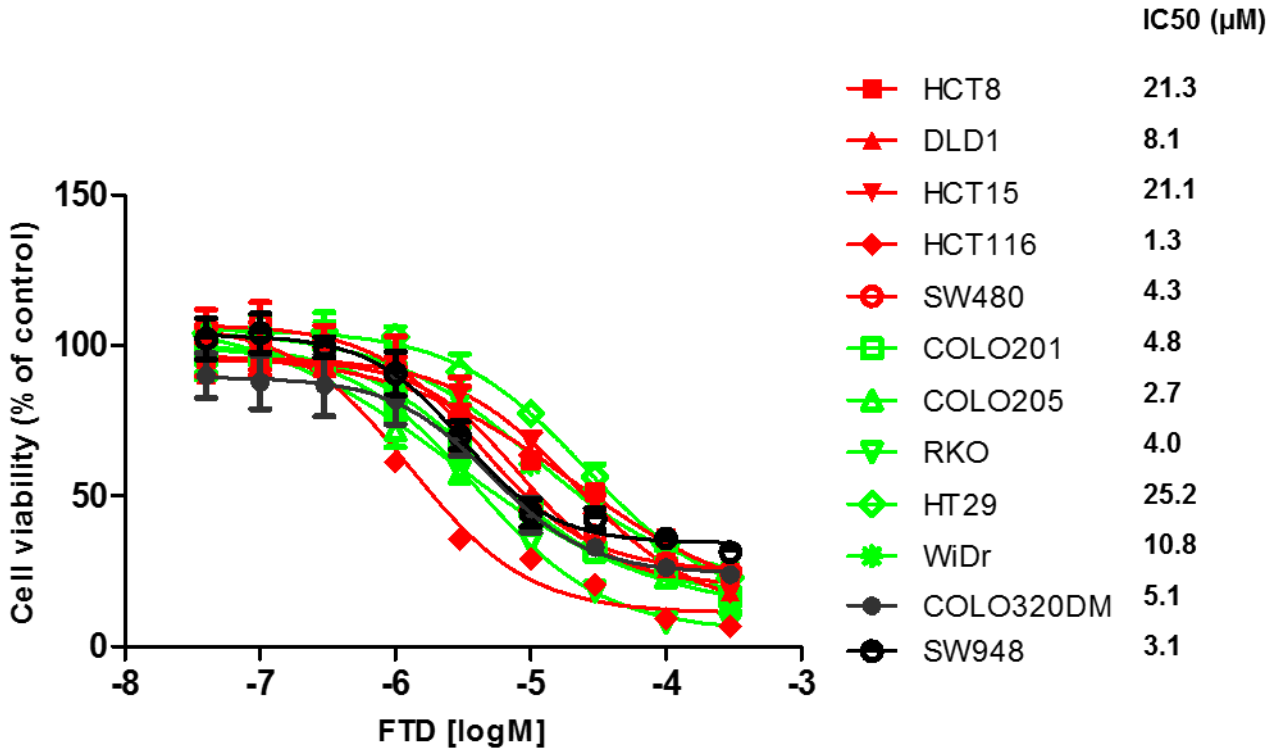

Figure 6. FTD inhibits cell proliferation of various colon cancer cell lines, irrespective of the *KRAS* and *BRAF* mutation statuses. Cell viability of various colon cancer cell lines. Values represent the mean cell viability (% of control). Error bars, standard deviation. Red symbols, cell lines with *KRAS* G12 or G13 mutations. Green symbols, cell lines with *BRAF* V600E mutations. Black symbols, cell lines with wild-type *KRAS* and *BRAF*.

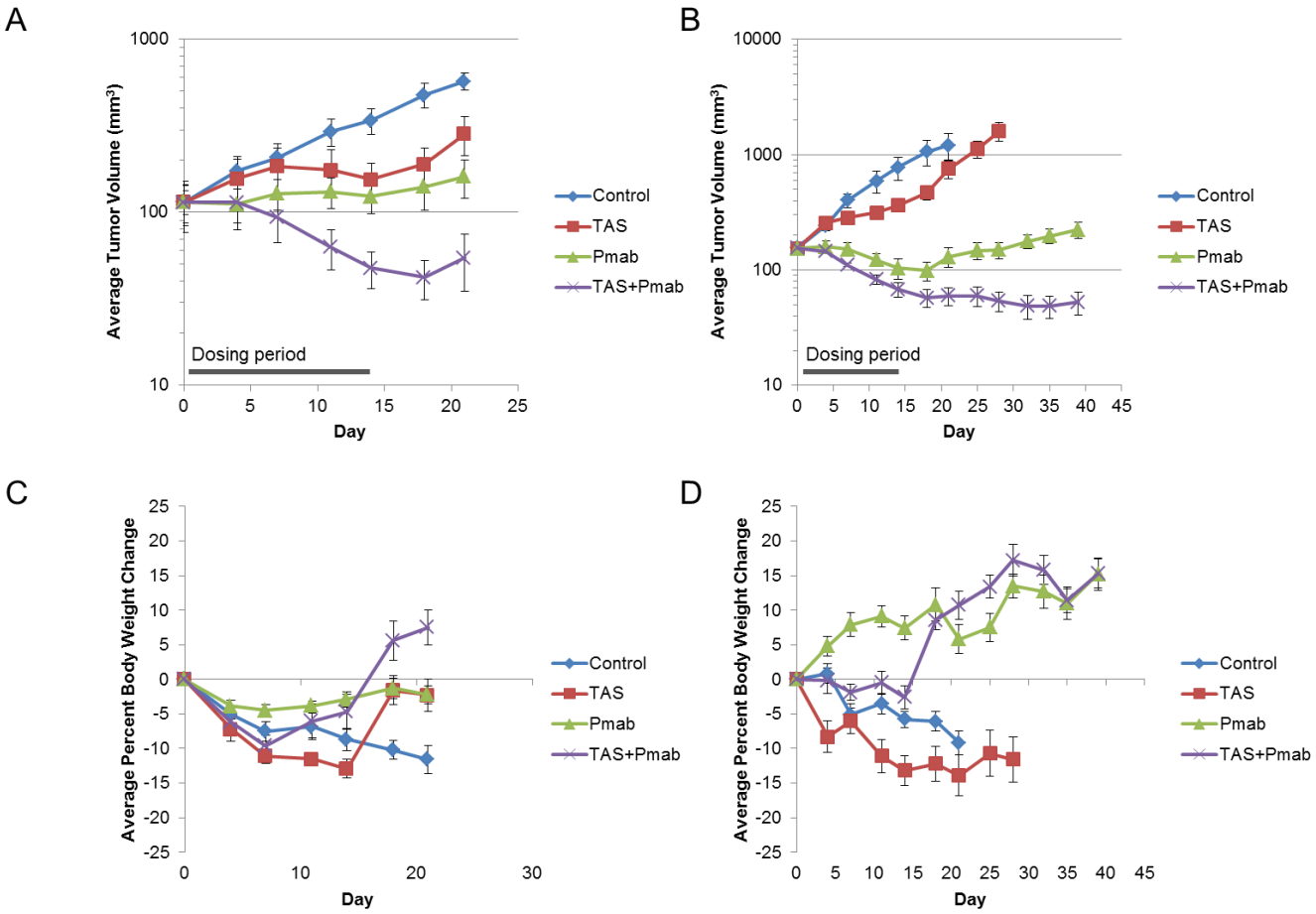

Figure 7. Co-administration of panitumumab (Pmab) and TAS-102 induces tumor regression *in vivo*. Antitumor effects and animal weights of Pmab, TAS-102, and Pmab/TAS-102 combination on the growth of subcutaneous LIM1215 (A, C) and COL-01-JCK (B, D) tumor xenografts. The mice were orally administered Pmab (3 mg/kg, twice weekly; intraperitoneally), TAS-102 (75 mg/kg, twice daily on a 5-days-on/2-days-off schedule; orally), or a combination of both agents for 2 weeks (from days 1 to 14). The data (A, B) represent the mean tumor volume ± standard error of the mean (n = 5). The values (C, D) represent the mean body weight change (% of initial body weight) ±standard error of the mean (n = 5).

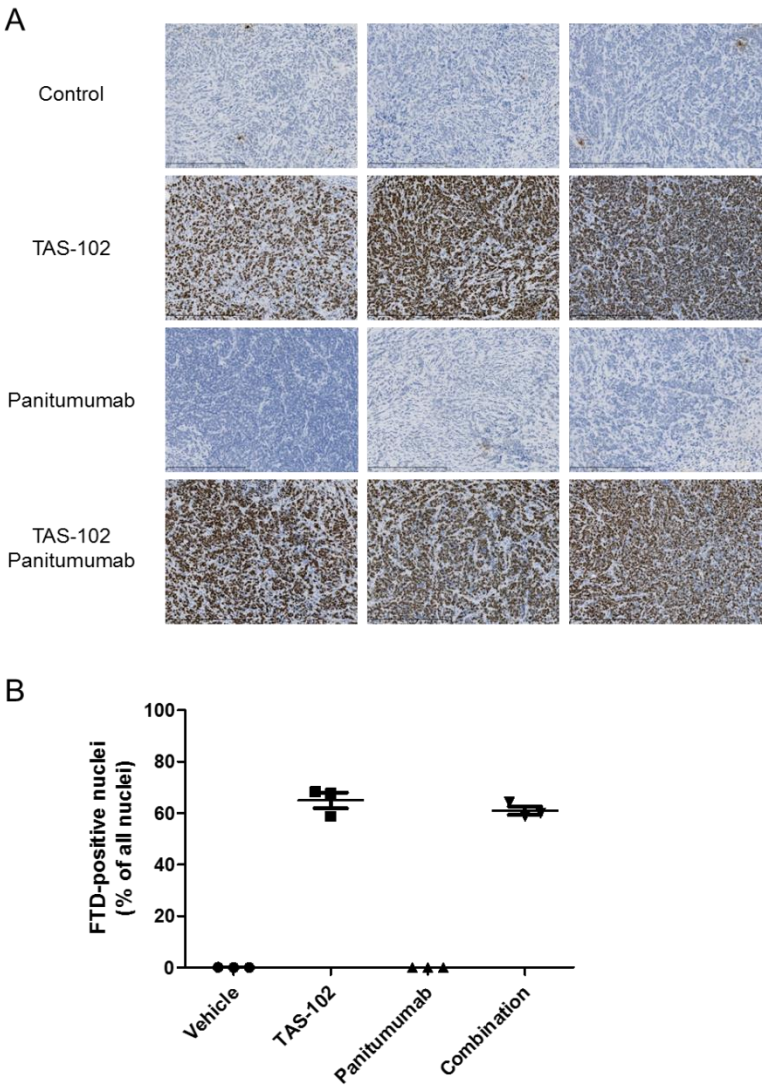

Figure 8. Immunohistochemical staining for FTD incorporated into DNA in the LIM1215 tumor xenograft model. LIM1215 tumor-bearing mice were administered TAS-102 alone, panitumumab alone, or the combination for 4 days (n = 3). Tumors were excised 24 h after the last treatment. Immunohistochemical staining (A) for the FTD incorporated into DNA was performed with an anti-BrdU antibody. Brown DAB staining indicates FTD-positive nuclei. Percentage of FTD-positive nuclei (B) was determined by image analysis. An unpaired t-test was used to compare TAS-102 alone and TAS-102/panitumumab combination treatments (p = 0.3197).

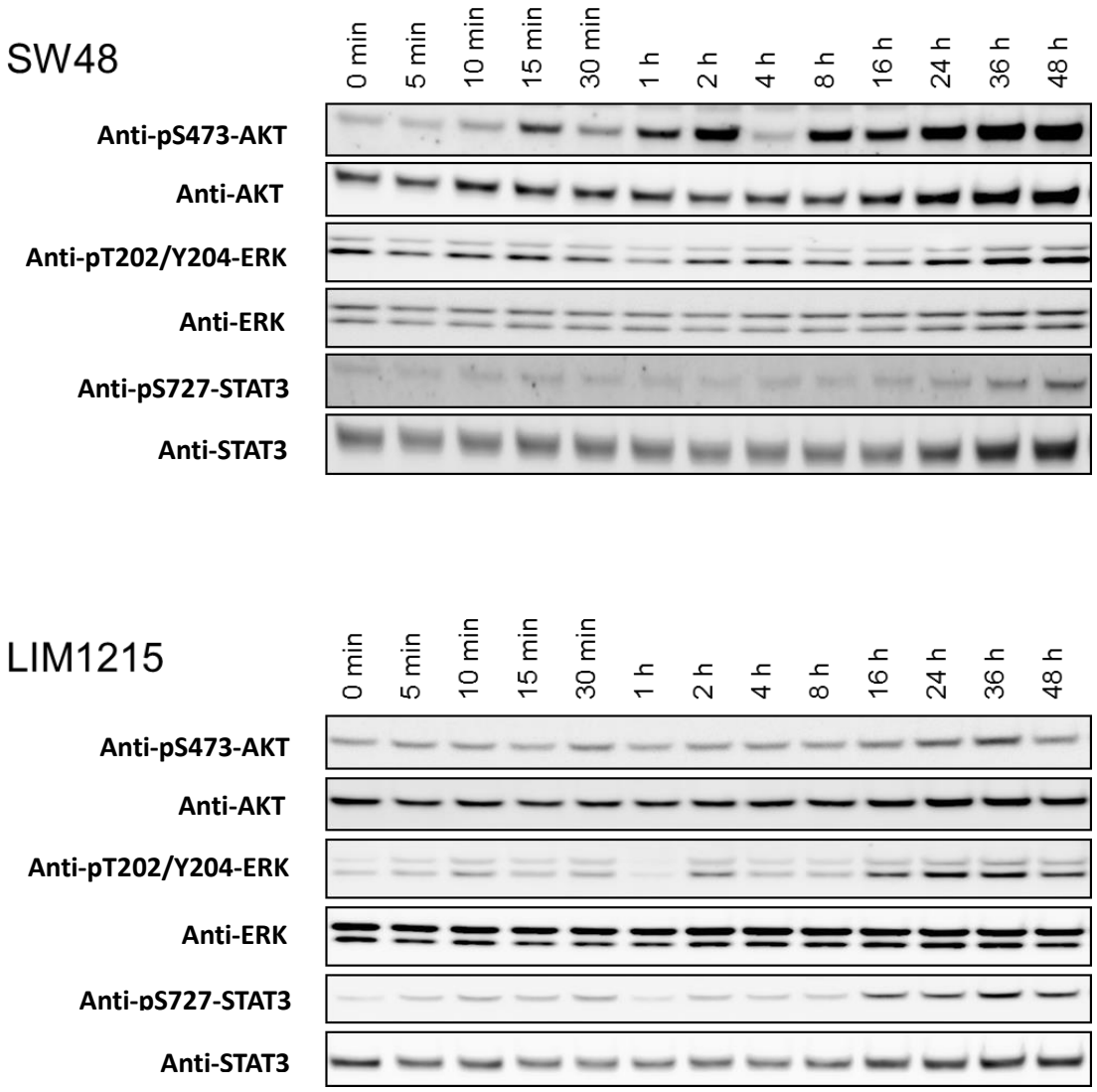

Figure 9. FTD-induced phosphorylation of AKT, ERK1/2, and STAT3 in SW48 and LIM1215 cells. SW48 (upper panel) and LIM1215 (lower panel) cells were treated with 3 μM FTD for the indicated times. Cells were then washed with cold PBS and lysed in a lysis buffer, which contained phosphatase and protease inhibitors. Equal amounts of protein were subjected to western blotting.

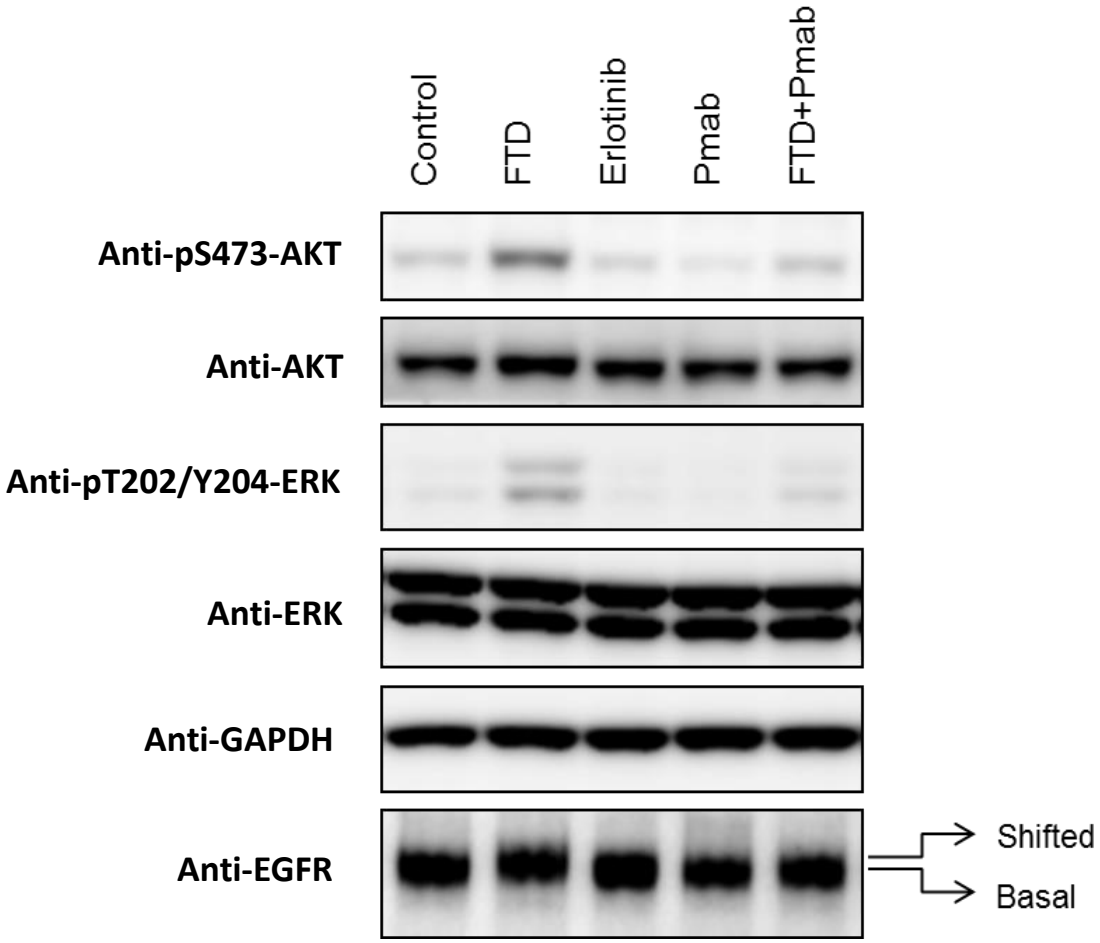

Figure 10. Panitumumab reverses FTD-induced ERK1/2 and AKT phosphorylation and EGFR gel mobility shift in LIM1215 cells. LIM1215 cells were seeded onto a 6-well plate and cultured for 24 h. The cells were subsequently treated with FTD (3 μM), panitumumab (100 ng/mL), erlotinib (10 μM), or a combination of FTD and panitumumab for 24 h, followed by western blotting analyses. FTD-induced band mobility shift of EGFR is indicated as "Shifted" versus "Basal". GAPDH was used as a loading control. The blots are representative of two independent experiments.

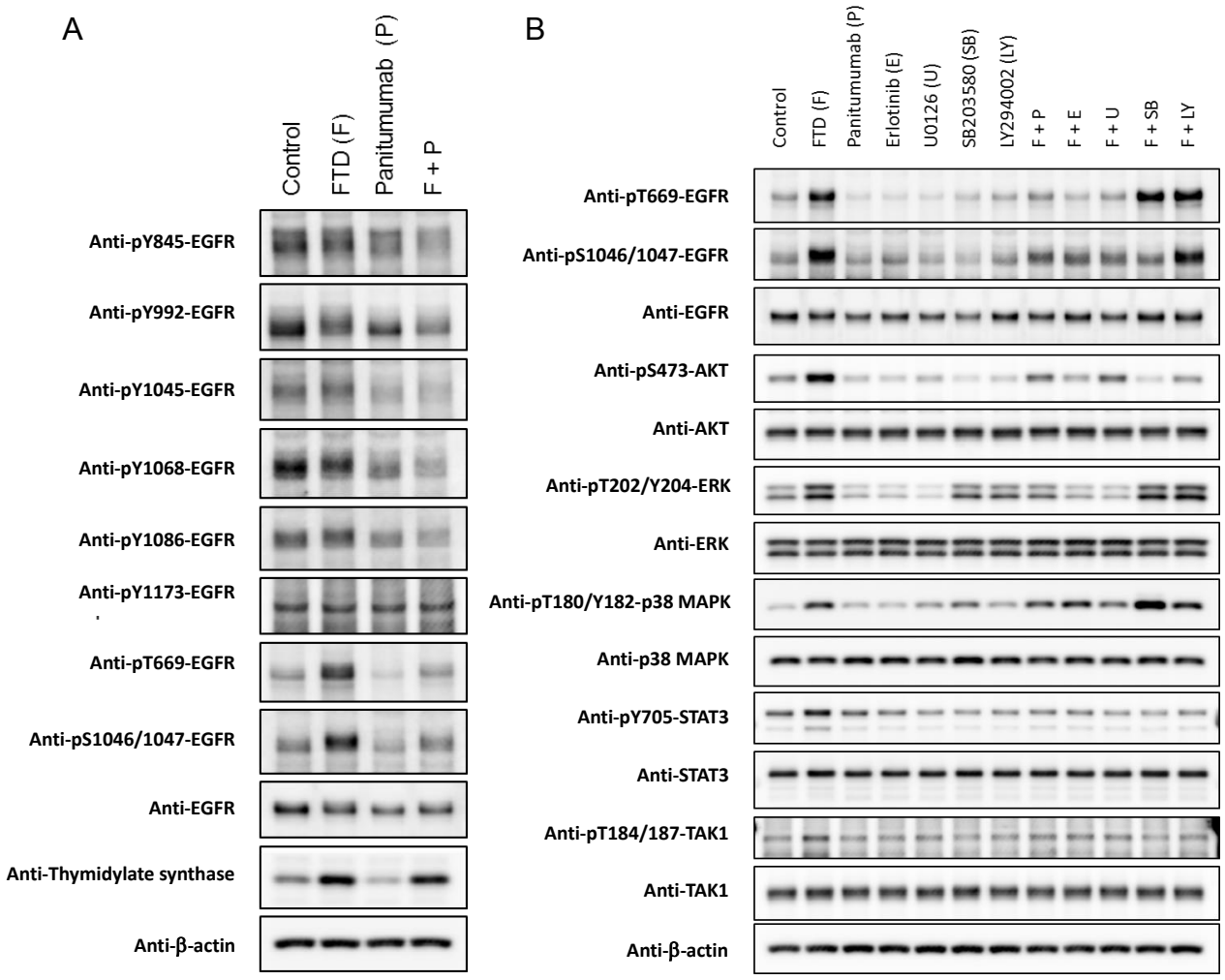

Figure 11. The effects of panitumumab and other kinase inhibitors on FTD-induced phosphorylation of EGFR and intracellular kinases in LIM1215 cells. LIM1215 cells were seeded onto 6-well plates and cultured for 24 h. EGFR phosphorylation (A) at specific residues was probed with each phospho-specific EGFR antibody following a 24-h treatment with FTD (3 μM), panitumumab (100 ng/mL), or their combination. Induction of thymidylate synthase expression was used as a marker of pharmacodynamic response to FTD. β-Actin was used as a loading control. LIM1215 cells (B) were treated for 24 h with FTD (3 μM), panitumumab (100 ng/mL), the EGFR tyrosine kinase inhibitor erlotinib (1 μM), MEK inhibitor U0126 (10 μM), p38 MAPK inhibitor SB203580 (10 μM), PI3K inhibitor LY294002 (10 μM), or their combinations as indicated.

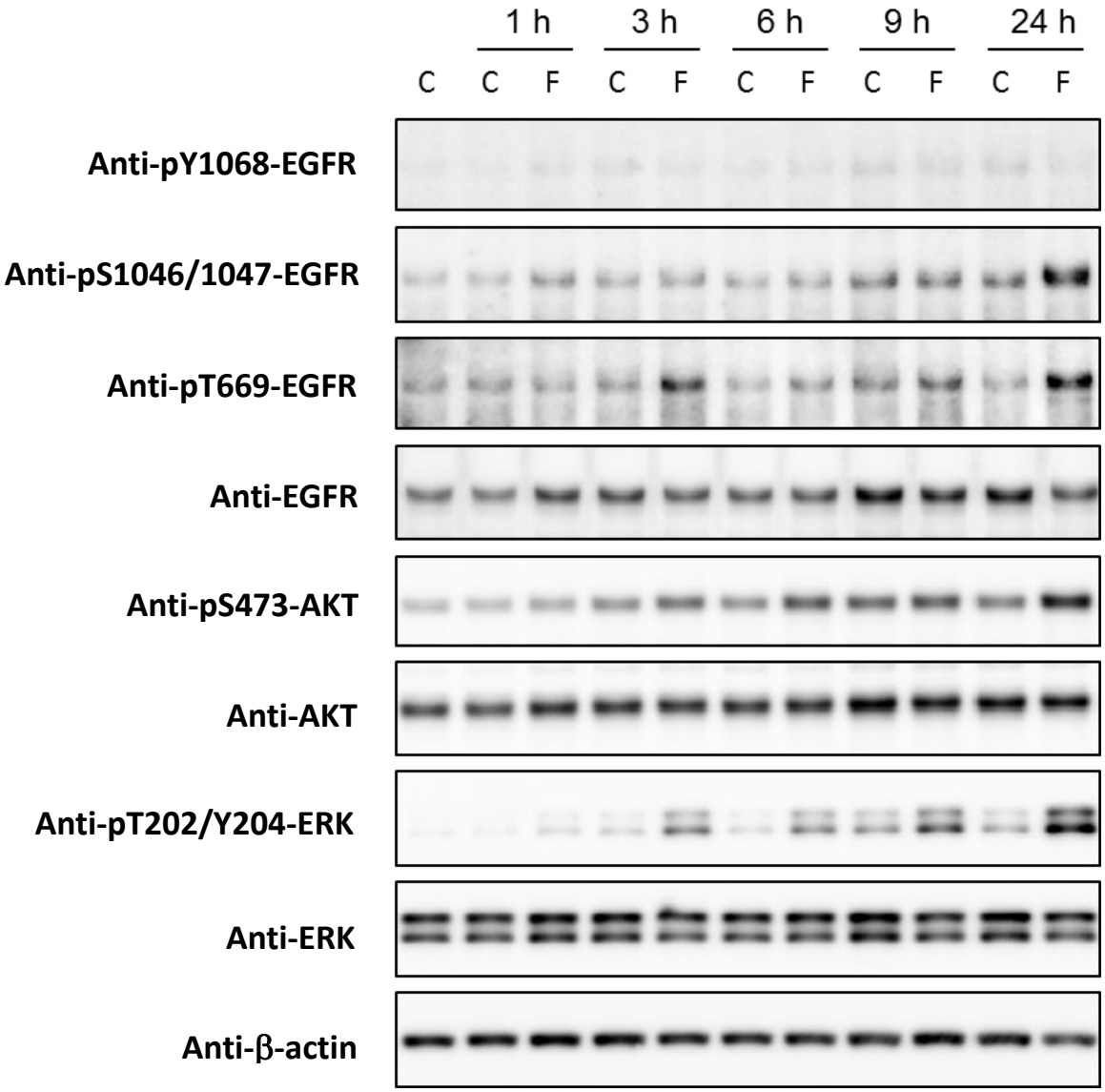

Figure 12. Time dependency of FTD-induced AKT/ERK/STAT3 and EGFR serine/threonine phosphorylation. LIM1215 cells were treated with DMSO or 3 μM FTD for the indicated times. Cells were then washed with cold PBS and lysed in a lysis buffer, which contained phosphatase and protease inhibitors. Equal amounts of protein were subjected to western blotting.

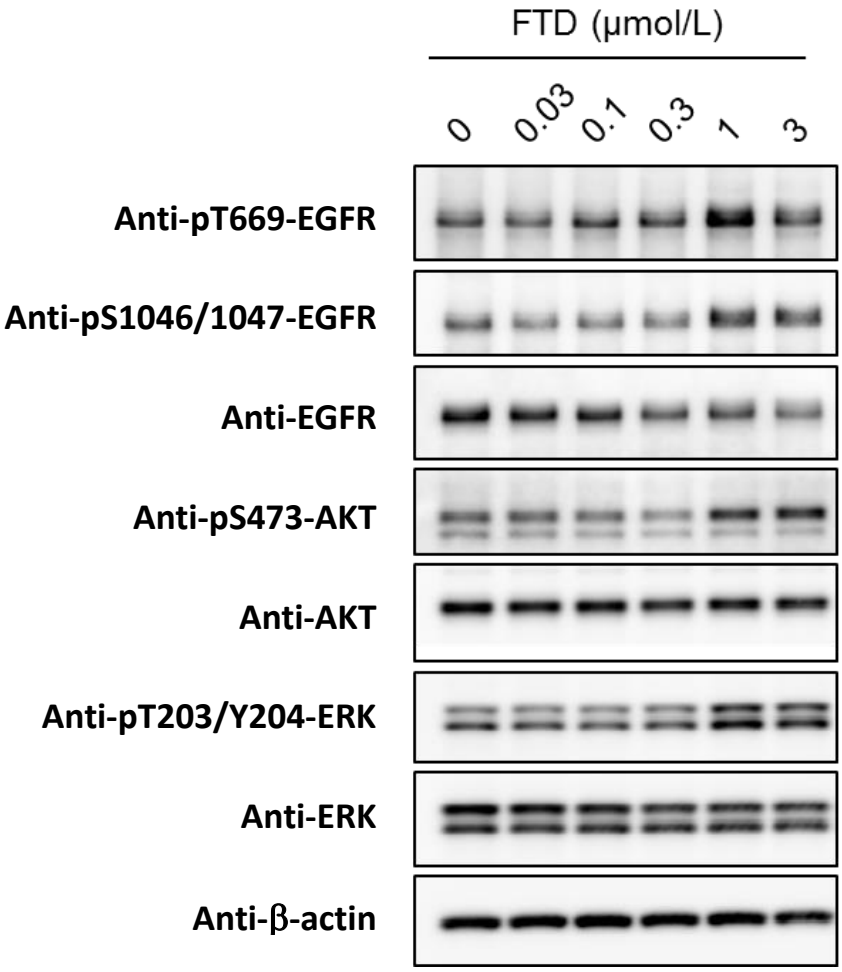

Figure 13. Concentration dependency of FTD-induced AKT, ERK1/2, and EGFR serine/threonine phosphorylation. LIM1215 cells were treated with FTD at the indicated concentrations for 24 h. Cell lysates were prepared and subjected to western blotting.

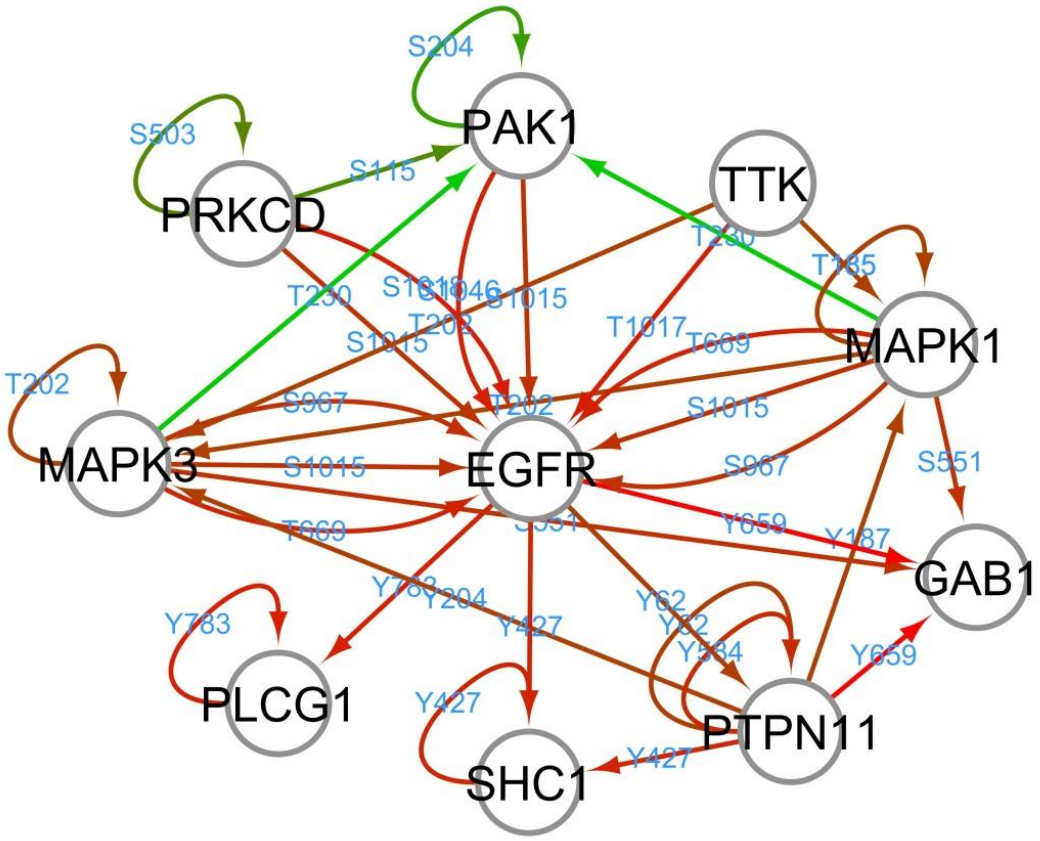

Figure 14. A highly connected subnetwork within EGFR and first neighbors. Each node is labeled with the gene symbols of the kinase and substrate. Kinases and their substrates are connected with edges (arrows). Labels on the edges indicate phosphorylation sites on the substrates. Inducible effects of FTD treatment on phosphorylation are shown in red, while suppressive effects are shown in green. The darker the color of the edges, the more significant effects the FTD treatment had.

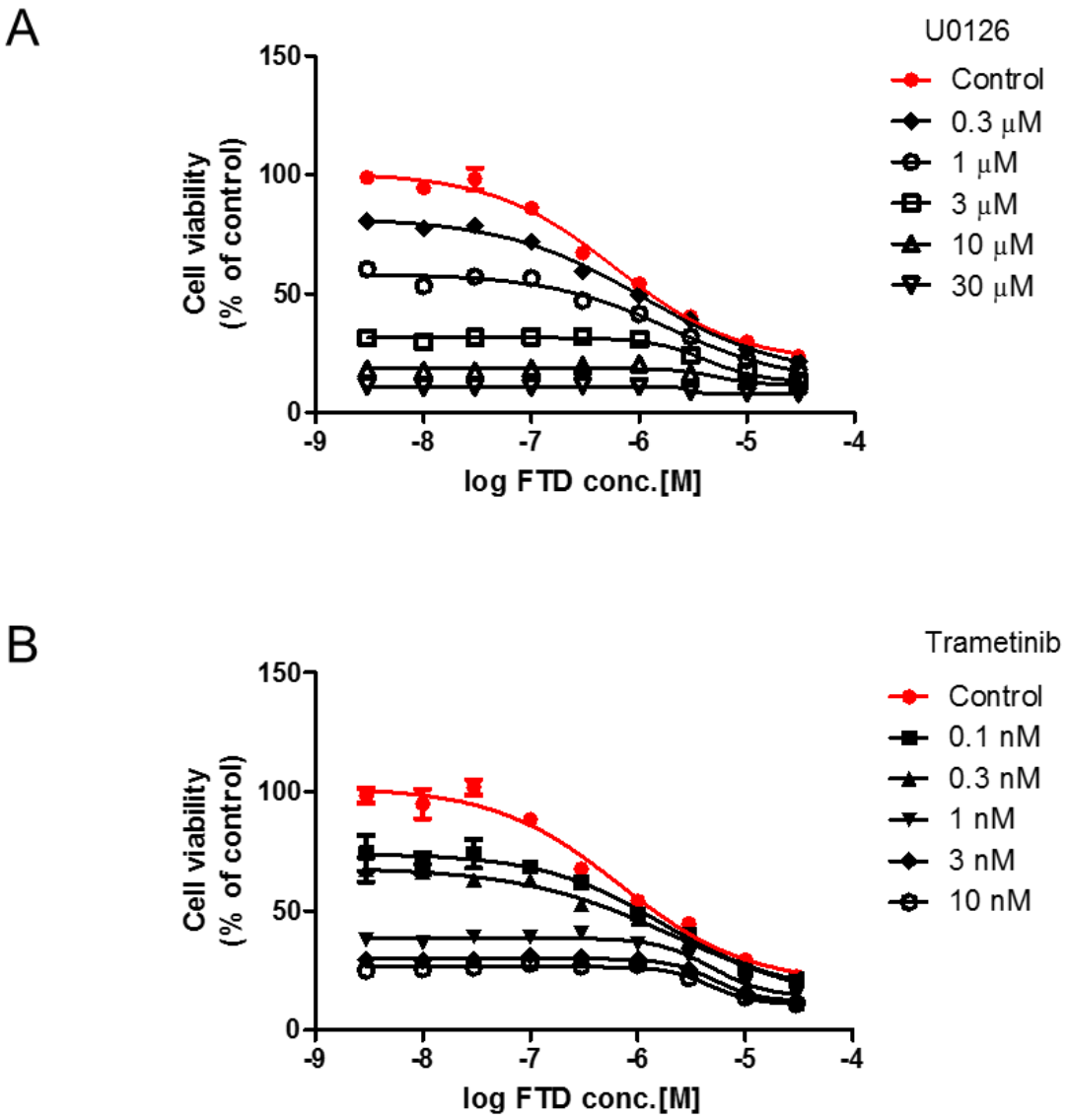

Figure 15. Combination treatment of FTD with MEK inhibitors shows additive antiproliferative effects in LIM1215 cells. The viability of LIM1215 cells was determined after co-treatment with FTD and U0126 (A) or FTD and trametinib (B) for 72 h.

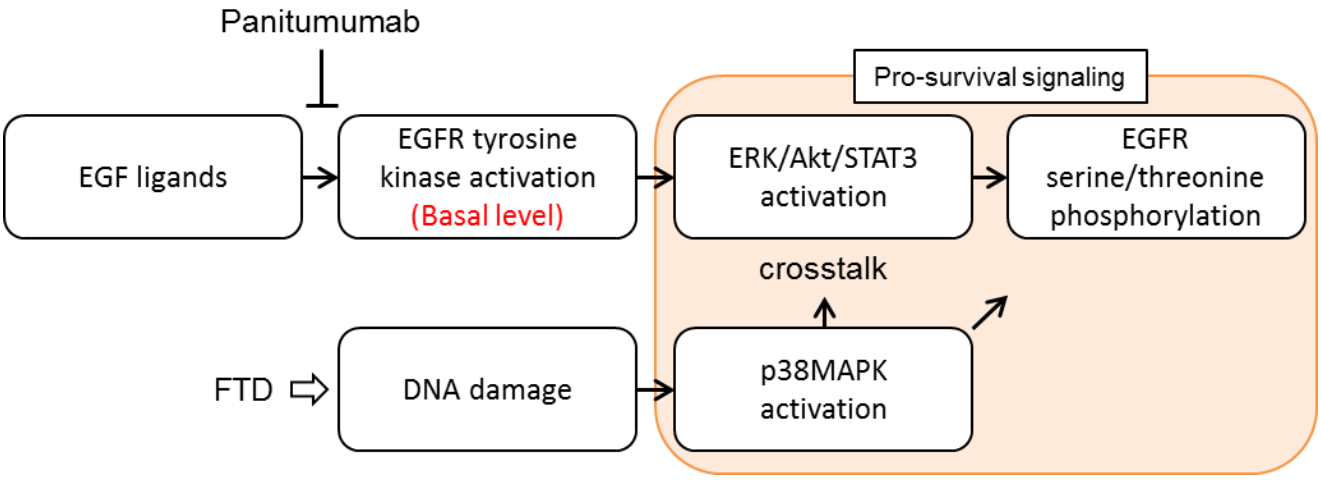

Figure 16. Schematic diagram of FTD-induced prosurvival signals. FTD induces DNA damage, which in turn elicits p38 MAPK activation. p38 MAPK signaling interacts with the signaling mediated by the basal activity of the EGFR tyrosine kinase through ERK/AKT/STAT3, promoting prosurvival signaling. EGFR serine/threonine phosphorylation occurs downstream of ERK/AKT/STAT3. Panitumumab inhibits the basal activity of EGFR, subsequent ERK/AKT/STAT3 activation, and EGFR serine/threonine phosphorylation, thereby making cells more sensitive to FTD-induced DNA damage.

Chapter 2

Biologic response of colorectal cancer xenograft tumors to sequential treatment with panitumumab and bevacizumab

Abstract

Recent studies in rat sarcoma GTPase (*RAS*) wild-type (WT) metastatic colorectal cancer (mCRC) suggest that the survival benefits of therapy using anti-epidermal growth factor receptor (anti-EGFR) and anti-vascular endothelial growth factor (anti-VEGF) antibodies combined with chemotherapy are maximized when the anti-EGFR antibody is given as first-line, followed by subsequent anti-VEGF antibody therapy. I reported reverse-translational research using LIM1215 xenografts of *RAS* WT mCRC to elucidate the biologic mechanisms underlying this clinical observation. Sequential administration of panitumumab then bevacizumab (PB) demonstrated a stronger tendency to inhibit tumor growth than bevacizumab then panitumumab (BP). Cell proliferation was reduced significantly with PB ($p < 0.01$) but not with BP based on Ki-67 index. Phosphoproteomic analysis demonstrated reduced phosphorylation of EGFR and EPHA2 with PB and BP compared with control. Western blotting showed reduced EPHA2 expression and S897-phosphorylation with PB; RSK phosphorylation was largely unaffected by PB but increased significantly with BP. In quantitative real-time PCR analyses, PB significantly reduced the expression of both lipogenic (*FASN, MVD*) and hypoxia-related (*CA9, TGFBI*) genes versus control. These results suggest that numerous mechanisms at the levels of gene expression, protein expression, and protein phosphorylation may explain the improved clinical activity of PB over BP

in patients with *RAS* WT mCRC.

Introduction

Potential benefit with anti- epidermal growth factor receptor (EGFR) antibodies appears to be limited to patients with rat sarcoma GTPase (*RAS*) wild-type (WT) metastatic colorectal cancer (mCRC)[72-74]; such patients had improved clinical outcomes when treated with an anti-EGFR antibody and chemotherapy as first-line therapy than when compared with an anti-VEGF antibody and chemotherapy[75]. RAS is a small guanosine triphosphate hydrolase that is constitutively activated by mutation in ~20% of human cancers[76]. *KRAS* is the predominantly mutated isoform in CRC[76]; 55.9% of patients with CRC harbor a *RAS* (*KRAS/NRAS*) mutation[77]. Constitutive RAS activation facilitates oncogenesis through the upregulation of signaling pathways such as mitogen-activated protein kinase (MAPK) and AKT[78,79]. *Post-hoc* analysis of the FIRE-3 study, in which patients with *RAS* WT mCRC received treatment with FOLFIRI plus cetuximab or bevacizumab, highlighted a durable overall survival (OS) advantage for the group of patients that received FOLFIRI and cetuximab as first-line therapy compared with FOLFIRI and bevacizumab (median 33.1 vs. 25.0 months; hazard ratio [HR] 0.70; p = 0.0059)[75]. There have also been indications that first-line therapy in *RAS* WT mCRC can determine the efficacy of subsequent treatments and affect outcomes[80-82]. Furthermore, an exploratory analysis of data from three randomized studies of mCRC suggested a trend towards improved OS with a first-line anti-EGFR

antibody plus chemotherapy followed by a second-line anti-VEGF antibody compared with the opposite sequence[83].

While the use of anti-EGFR antibody in first-line treatment can increase the efficacy of second-line anti-VEGF antibodies[84,85], initial treatment with an anti-VEGF antibody may decrease the efficacy of subsequent anti-EGFR antibodies[86-88]; a sufficient anti-VEGF antibody-free period prior to treatment with second-line anti-EGFR antibodies is necessary to limit this reduced efficacy[89]. The biologic rationale for this finding remains unknown, but mechanisms have been suggested that may contribute[81,82]. *RAS* WT mCRC tumor cells that develop resistance to an anti-EGFR antibody may retain sensitivity to an anti-VEGF antibody, but resistance to an anti-VEGF antibody can lead to the development of resistance to anti-EGFR antibodies[81,82]. Indirect evidence for this comes from the finding that resected liver metastases from Japanese patients with mCRC treated with bevacizumab demonstrated significantly increased tumoral *VEGFA* mRNA expression[90], while in pre-clinical models of CRC, overexpression of *VEGFA* or treatment with exogenous VEGF-A ligand conferred resistance to cetuximab[86,91]. Taken together, these findings highlight a potential mechanism of acquired resistance to anti-EGFR antibodies in mCRC that potentiates tumor angiogenic ability. Nevertheless, many details regarding the biologic mechanisms underlying the efficacy of the two different treatment sequences in the clinic are yet to

be explored.

Here, I present the results of reverse-translational research using xenograft models of human CRC to evaluate the biologic reasons for the improved outcomes seen with sequential use of an anti-EGFR antibody (panitumumab) followed by an anti-VEGF antibody (bevacizumab) compared with the opposite sequence in patients with *RAS* WT mCRC. I performed quantitative phosphoproteomic and transcriptome analyses of xenograft tumors to identify biological changes with sequential treatment that may provide some explanation for the survival benefits previously demonstrated in clinical settings.

Materials and Methods

Cells and reagents

The human colon cancer cell line LIM1215 was obtained from the European Collection of Authenticated Cell Cultures (ECACC, Salisbury, UK). LIM1215 cells were cultured in conditions recommended by the ECACC. Panitumumab was provided by Amgen (Thousand Oaks, CA, USA). Bevacizumab was purchased from Roche (Basel, Switzerland).

Xenograft construction and study treatment

All *in vivo* experimental protocols complied with the Guide for the Care and Use of Laboratory Animals (8th Edition), and were approved by the Institutional Animal Care and Use Committee of the Shonan Research Center (#00011823), Takeda Pharmaceutical Company Limited, or Shanghai Medicilon Inc. (Shanghai, China). LIM1215 cells were selected because they have WT *RAS (*WT *KRAS* and *NRAS)* and WT *BRAF*, and panitumumab and bevacizumab have previously shown anti-tumor effects in xenografts of LIM1215 tumors[92]. Six- to seven-week-old female C.B17/Icr-scid/scid Jcl (SCID) mice (from CLEA, Tokyo, Japan, or Beijing Vital River Animal Technology, Beijing, China) maintained under specific pathogen-free conditions were injected subcutaneously in the right flank with five million LIM1215 cells mixed with Matrigel (Corning, NY, USA). *In vivo* LIM1215 xenografts were constructed at two different sites,

LIM1215(A) and LIM1215(B). Once tumor volume reached 50–200 mm^3, mice were randomized to each treatment group. All treatment was intraperitoneal. The vehicle control group received saline twice-weekly for 2 weeks or 4 weeks. Panitumumab and bevacizumab were given twice-weekly at 3 mg/kg and 10 mg/kg, respectively. The panitumumab-bevacizumab (PB) group received panitumumab for 2 weeks followed by bevacizumab for 2 weeks; the bevacizumab-panitumumab (BP) group received the reverse sequence. One group received bevacizumab (BB) for 4 weeks and other groups received monotherapy with panitumumab (P group) or bevacizumab (B group) for 2 weeks (Fig. 17).Tumor volumes (length x $width^2$ x 0.5) were measured twice-weekly with Vernier calipers and antitumor activity was evaluated by percentage of relative growth rate (GR) calculated using the following equation: %GR = (mean growth rate of treated tumor/mean growth rate of vehicle control group) x 100. Following final tumor volume measurements, mice were anaesthetized 24 hours after final drug administration and euthanized by cervical dislocation, and tumor samples were collected. Samples from the LIM1215 (A) xenografts were used for the transcriptome and phosphoproteome analyses, and quantitative real-time PCR (qRT-PCR). The LIM1215 (B) xenograft samples were used for qRT-PCR, western blotting, and histology analyses.

Tumor tissue analyses

Formalin-fixed paraffin-embedded sections (4μm) of resected tumor tissue were used for histologic analysis. Hematoxylin and eosin staining was conducted according to standard protocol. Ki-67 staining was performed with anti-Ki-67 antibody (Nichirei Biosciences, Tokyo, Japan) and hematoxylin background. The Ki-67 index (%) was estimated by counting the number of Ki-67-positive cell nuclei per 1200–1800 tumor cells in the three regions of the tumor with the greatest staining density.

Phosphoproteomic analysis and western blotting

Quantitative phosphoproteomic analysis of xenografts was performed using mTRAQ technology (AB Sciex, Framingham, MA, USA). Xenografts were homogenized in homogenization buffer (10 mM phosphate [pH 7.5], 8 M urea, protease inhibitor, and phosphatase inhibitors) and proteins were precipitated with 5 volumes of acetone followed by resolution in lysis buffer (4% sodium dodecyl sulfate [SDS, SERVA Electrophoresis GmbH, Heidelberg, Germany], 0.4% 3-[3-cholamidopropyl] dimethylammoniopropanesulfonate [CHAPS, DOJINDO, Kumamoto, Japan] and 10 mM triethylammonium bicarbonate [TEAB, Wako, Osaka, Japan]). Each lysate, and a mixture of all lysates (internal standard), were digested with Lys-C (Wako, Osaka, Japan) and trypsin (Promega, Madison, WI, USA) by the FASP method[93] using Amicon Ultra-4 30k centrifugal filter units (Merck KGaA, Darmstadt, Germany). The digested peptides

were loaded onto TiO_2 chips (GL Science, Tokyo, Japan) for phosphopeptide enrichment, and phosphopeptides were labeled with mTRAQ reagent (AB Sciex, Framingham, MA, USA). Labeled phosphopeptides from each sample and the internal standard were mixed and separated into 12 fractions on a polysulfoethyl A SCX column (PolyLC, Columbia, MD, USA). The fractions were then analyzed using fusion mass spectrometry (MS) (Thermo Scientific, Waltham, MA, USA) coupled to a nano-liquid chromatography system (EASY-nLC 1000). MS files were processed with Proteome Discoverer 1.4 (Thermo Scientific, Waltham, MA, USA) using MASCOT (v. 2.5, Matrix Science, London, UK). The ratio of sample:vehicle was calculated by sample:mixture / vehicle:mixture.

For western blotting, RIPA buffer (Wako, Osaka, Japan) containing inhibitors (#78443, Thermo Scientific, Waltham, MA, USA) was added to the recovered tumor, and lysis was carried out using a bead homogenizer. The protein concentration of the supernatant was measured by BCA Protein Assay (Bio-Rad, Hercules, CA, USA). Tissue lysates were subjected to SDS-polyacrylamide gel electrophoresis (SDS-PAGE, Criterion TGX precast gels, Bio-Rad, Hercules, CA, USA) and transfer by Trans-Blot Turbo System (Bio-Rad, Hercules, CA, USA). Antibodies used were as follows: anti-ephrin type-A receptor 2 (EPHA2; #6997), anti-phospho-EPHA2 (S897; #6347), anti-ribosomal S6 kinase (RSK) (#8408), anti-phospho-RSK

(S380; #11989), and anti-β-actin (#5125) (all from Cell Signalling Technology, Danvers, MA, USA). Western blots were developed using ImmunoStar Zeta or ImmunoStar LD (Wako, Osaka, Japan). Band densities were quantified by an image analyzer (LAS-3000, Fujifilm, Tokyo, Japan).

Transcriptome analysis and qRT-PCR

Total RNA was extracted from tumor tissue and treated with DNase using the RNeasy Mini Kit (QIAGEN, Germantown, MD, USA) according to the manufacturer's recommendations. Gene expression analysis was conducted by microarray on SurePrint G3 Human GE 8X60k V3 Microarrays (Agilent, Santa Clara, CA, USA) according to the manufacturer's guidelines. Signal values were logarithmically transformed and subjected to quantile normalization. Statistical significance of the expression data was determined using fold change (above 1.5 fold) and independent T-test (p-value < 0.05) between two groups in array probes with Flag-P in both groups. Sets of differentially expressed genes (DEGs) were selected using the Omicsoft Array Studio (QIAGEN, Germantown, MD, USA). Enrichment analysis for DEG sets (Diseases and Bio Functions, Canonical Pathways) was performed using Ingenuity Pathway Analysis (QIAGEN, Germantown, MD, USA).

Purified RNA was reverse-transcribed with the High-Capacity cDNA Reverse Transcription Kit with RNase Inhibitor (Thermo Fisher Scientific, Waltham, MA, USA) and qRT-PCR was

performed with the TaqMan® Fast Advanced Master Mix (Thermo Fisher Scientific, Waltham, MA, USA) using a ViiA 7 Real-Time PCR System (Thermo Fisher Scientific, Waltham, MA, USA). Relative quantified RNA was normalized to the housekeeping gene β-actin, and results were evaluated using the comparative ΔΔCT method. The TaqMan® Gene Expression Assays (Thermo Fisher Scientific, Waltham, MA, USA) used for each gene are listed in Supplementary Table 4.

Statistical analyses

Data for vehicle controls and other groups was initially analyzed using Bartlett's test for homogeneity of variance. When variance was homogenous, differences between groups were analyzed by Dunnett's multiple comparison test. When variance was not homogenous, the Steel-Dwass multiple comparison test was used. A significance level of $p < 0.05$ was used.

Results

PB was more effective than BP at inhibiting tumor growth rate in xenograft models

In the LIM1215 (A) xenograft, panitumumab and bevacizumab alone demonstrated almost equivalent efficacy (Fig. 18A). Obvious growth retardation was observed in all sequential treatment groups (Fig. 18B). Relative GR was significantly reduced with PB, BP, and BB in LIM1215 (A) xenografts compared with vehicle control and there was a numerically greater decrease in growth rate in the PB group than in the BP group (Fig. 18C). A significant decrease in relative GR was also apparent in the PB group in LIM1215 (B) xenografts (Fig. 19).

Ki-67 index fell with PB

Cell proliferation per Ki-67 index was significantly reduced with PB compared with vehicle controls (66.5% vs. 75.8% Ki-67 positive cells, $p < 0.01$; Fig. 20E). Proliferation was also numerically reduced compared with vehicle controls using BP (72.0% Ki-67 positive cells), but to a lesser extent than with PB. The BB treatment sequence did not have an antiproliferative effect (78.1% Ki-67 positive cells) (Fig. 20).

EGFR and EPHA2 phosphorylation Levels were reduced with PB and BP.

Table 5 shows the phosphopeptides selected from all phosphoproteomic analysis data according to the following criteria: 1, the peptide is a part of growth factor receptor; 2,

phosphorylation of the site has previously been identified by a site-specific method (i.e. methods other than omics); 3, signals were detected in all 4 groups (vehicle control, PB, BP, and BB).

Levels of phosphorylated growth factor receptors (EGFR and EPHA2) were reduced with both PB and BP compared with vehicle control (Table 5); changes in insulin-like growth factor 2 receptor were small in all groups. However, PB demonstrated greater reductions in the phosphorylation level of EGFR and EPHA2 than BP. The greatest change was demonstrated for EPHA2 pS897 and EPHA2 pS901; in the PB group, expression was 36% and 42%, respectively, of the level in vehicle controls compared with 77% and 68%, respectively, in the BP group. Treatment with BB did not result in a decrease in the levels of phosphorylated EPHA2 compared with vehicle control, with only slight reductions in phosphorylation of EGFR at S991 and S1166 (Table 5).

EPHA2 protein expression and serine phosphorylation were decreased by PB, and RSK phosphorylation was increased with BP

EPHA2 was selected for study by western blotting due to its strong inhibition with PB, as demonstrated in phosphoproteomic analysis. Western blotting showed reduction of total EPHA2 protein and EPHA2 S897-phosphorylation (pEPHA2) levels by PB, while BP showed large individual variation; BB had little effect (Fig. 21A and B). Compared with vehicle controls, the pEPHA2:EPHA2 ratio was reduced significantly with PB ($p < 0.01$) (Fig. 21C and D). The

pEPHA2:EPHA2 ratio was also reduced with BP, but with less effect than PB (Fig. 21C).

Due to the known ability of RSK to induce pEPHA2 in a ligand-independent manner[16,20,94], RSK was also selected for study by western blotting. PB had minimal effect on both levels of total RSK1 protein and RSK S380-phosphorylation (pRSK) compared with vehicle control. Conversely, both BP and BB increased pRSK levels compared with vehicle control (Fig. 21E and F). The pRSK:RSK ratio was significantly increased by both BP ($p < 0.001$) and BB ($p < 0.01$) (Fig. 21G and H).

Variable lipogenic gene expression was observed with sequential treatment

Significant changes in pathway activity relating to lipid metabolism occurred in tumors treated with BB (Table 6) and expression levels of some lipogenic genes were higher with BB versus vehicle control (Table 7). Some pathways were changed in the PB and BP groups, and with panitumumab alone, which altered pathways related to lipid metabolism (Table 8).

Lipogenic and hypoxia-related gene expression was reduced with PB

qRT-PCR analysis was performed for lipogenic genes based on the results of transcriptome analysis and demonstrated a definite change in lipid metabolism. Significant suppression of the lipogenic genes fatty acid synthase (*FASN*) and mevalonate diphosphate decarboxylase (*MVD*) was demonstrated with treatment using panitumumab alone, but no suppression was apparent with

bevacizumab alone (Fig. 22A and *C*). Furthermore, expression levels of *FASN* (59% of expression vs.control, $p < 0.01$) and *MVD* (56% of vs. control, $p < 0.05$) were significantly decreased in the PB group compared vehicle controls, and 3-hydroxy-3-methylglutaryl-CoA reductase (*HMGCR*) and lanosterol synthase (*LSS*) were numerically decreased (Fig. 22E to H). For the hypoxia-related genes carbonic anhydrase 9 (*CA9*) and transforming growth factor-beta induced protein (*TGFBI*), the P group showed significant suppression, but the B group did not demonstrate suppression (Fig. 22I and J). Furthermore, expression of *CA9* (22% expression vs. control; $p < 0.01$) and *TGFBI* (11% expression vs.control; $p < 0.01$) were significantly reduced compared with control using PB (Fig. 22K and L). In the BP group the expression of all studied genes was reduced, but none of the reductions were statistically significant. Although transcriptome analysis (LIM1215[A]) had indicated an increase in lipid metabolism pathways in the BB group, quantitative PCR (LIM1215[B]) did not demonstrate enhanced expression of lipogenic genes in this treatment group.

Discussion

Anti-EGFR antibodies and anti-VEGF antibodies represent the current standard of care for front-line mCRC treatment when used in combination with cytotoxic chemotherapy regimens[3,6]; however, evidence suggests that the sequence in which these agents are given to patients may affect clinical outcomes[80-89]. In this study, using xenograft models of *RAS/BRAF* WT CRC, PB was found to be the most efficacious treatment sequence with regards to relative GR and reducing the Ki-67 index of tumor cells; the opposite sequence failed to achieve significant reduction of Ki-67 index. Phosphoproteomic analysis also showed that PB was the more effective treatment sequence with regards to reducing the phosphorylation status of key cancer-related signaling proteins, including EGFR and EPHA2, with 36% EPHA2 (pS897) phosphorylation with PB versus vehicle control. Western blot experiments confirmed that overall EPHA2 levels and the pEPHA2:EPHA2 ratio were significantly reduced with PB, but not BP or BB, which indicates that PB reduces the phosphorylation status of EPHA2 by mechanisms other than reduction of overall EPHA2 levels.

In this study, the effect of BP could be influenced by the negative impact of bevacizumab on subsequent anti-EGFR efficacy in mCRC, as previously demonstrated in retrospective clinical studies[86-89]. Derangère et al. demonstrated a significant PFS advantage for patients with *RAS* WT mCRC receiving second- or third-line anti-EGFR antibodies after non-bevacizumab therapy

compared with prior bevacizumab (4.0 vs. 2.8 months; p = 0.003)[86]. Similarly, a study of patients with *KRAS* exon 2 WT mCRC undergoing anti-EGFR therapy following failure of fluoropyrimidines, oxaliplatin, and irinotecan demonstrated significantly longer PFS and OS and improved response rates for patients who had received bevacizumab more than 6 months prior to anti-EGFR therapy compared with less than 6 months before (PFS 6.6 vs. 4.2 months, p = 0.038; OS 14.3 vs. 11.6 months, p = 0.039; response rate 47.5% vs. 24.3%, p = 0.012)[89]. While such retrospective studies require validation in prospective settings, the findings are consistent with those of the current study.

Treatment with bevacizumab enhances *VEGFA* gene expression in CRC tumors and subsequently increases VEGF-A protein concentrations in the blood[86,90], which in turn is suggested to cause resistance to anti-EGFR antibodies[86]. Similarly, a study using SUM149 xenografts identified a significant reduction in the targeting of radiolabeled cetuximab to tumors following bevacizumab treatment[95]. Alongside my findings, and considering the shared molecular target of cetuximab and panitumumab, such studies suggest biologic mechanisms that may account for the reduced clinical efficacy of anti-EGFR antibodies when administered following an anti-VEGF antibody in mCRC.

Panitumumab suppresses EGFR signaling, preventing transcriptional activation of EPHA2

through MAPK signaling[96,97]. This may explain both the significant reduction in Ki-67 index and reduced expression of EPHA2 that I identified with PB versus vehicle controls. Increased EPHA2 expression in CRC predicts poor response to cetuximab[98,99]. Moreover, S897 phosphorylation of EPHA2 can be induced in a ligand-independent manner by RSK[16,20,94], AKT[21] or PKA[100]. BP and BB increased RSK phosphorylation compared with vehicle controls; this may be related to the hypoxic response following inhibition of angiogenesis by bevacizumab[101] and subsequent induction of RSK hyperphosphorylation[102].

In terms of gene expression, PB was the only treatment sequence to induce statistically significant reductions in both lipogenic and hypoxia-related genes in my xenograft models (LIM1215[B]). Moreover, changes in the lipogenic genes *FASN, HMGCR*, *MVD*, and *LSS* were also demonstrated in this study. Significant suppression of *FASN* and *MVD* expression was observed with PB, which may indicate anti-tumor activity; reduced activity of lipogenic pathways is suggested to reduce malignancy and suppress oncogenic proliferation[103]. Inhibition of EGFR signaling by panitumumab may lead to functional inhibition of sterol regulatory element binding proteins, thereby reducing expression of lipogenic genes[104,105]. Given that hypoxia is known to induce the expression of lipogenic genes[106], the expression of the hypoxia-related genes *TGFBI* and *CA9* was examined. PB significantly reduced the expression of *CA9* and *TGFBI*, indicative of

reduced hypoxic response in the tumor environment. Without therapeutic intervention, hypoxia-inducible factor-1 (HIF-1) is constantly induced in hypoxic tumors and promotes malignant processes. The demonstrated reduction in *CA9* expression is thought to be due to panitumumab-mediated suppression of HIF-1 transcriptional activity or HIF-1 protein expression[107-109]. TGFBI protein is another prognostic factor in CRC[110] thought to be involved in activation of cell proliferation, adhesion, migration, and invasion _ENREF_110[111-114]. Therefore, reduced *TGFBI* expression, as demonstrated by PB in the current study, may contribute to the suppression of tumor progression in the clinic.

In summary, PB has improved activity versus BP in terms of inhibition of tumor growth, reduction of tumor cell proliferation index, reduced expression and phosphorylation status of EPHA2, and downregulation of expression of lipogenic and hypoxia-related genes. Taken together, these findings may explain in part the reason for the survival benefits previously demonstrated in the clinical settings for the use of first-line anti-EGFR antibodies followed by anti-VEGF antibodies compared with first-line anti-VEGF antibodies followed by anti-EGFR antibodies[81-83].

Tables and Figures

Table 4. TaqMan® Gene Expression Assays used for Measurement of each Gene.

Gene symbol	Gene name	Assay ID
CA9	Carbonic anhydrase 9	Hs00154208_m1
TGFBI	Transforming growth factor-beta induced	Hs00932747_m1
MVD	Mevalonate disphosphate decarboylase	Hs00964565_m1
LSS	Lanosterol synthase	Hs01552331_m1
FASN	Fatty acid synthase	Hs01005622_m1
HMGCR	3-hydroxy-3-methylglutaryl-CoA reductase	Hs00168352_m1
ACTB	Actin beta	Hs01060665_g1

Table 5. Levels of Phosphorylated Growth Factor Receptors in LIM1215(A) Xenografts Treated with PB, BP, and BB Relative to Vehicle Control. B, bevacizumab; P, panitumumab.

Protein name	Phosphorylation site	Fold change vs. vehicle control		
		PB	BP	BB
EGFR	pT693 (pT669)	0.60	0.70	1.04
	pS991 (pS967)	0.59	0.71	0.82
	pS1166 (pS1142)	0.81	1.02	0.81
EPHA2	pS897	0.36	0.77	1.07
	pS901	0.42	0.68	1.43
IGF2R	pS2049	0.89	0.84	0.95
	pS2484	1.02	0.91	0.89

Table 6. Enrichment Analysis of LIM1215(A) Xenografts Treated with Bevacizumab -Bevacizumab Compared with Vehicle Control (all Canonical Pathways, $p < 0.001$).

Canonical pathways	**p-value**
Superpathway of cholesterol biosynthesis	1.3E-18
Cholesterol biosynthesis I	3.2E-12
Cholesterol biosynthesis II (via 24,25-dihydrolanosterol)	3.2E-12
Cholesterol biosynthesis III (via Desmosterol)	3.2E-12
Mevalonate pathway I	3.8E-08
Superpathway of Geranylgeranyldiphosphate biosynthesis I (via Mevalonate)	1.8E-07
Gamma-linolenate biosynthesis II (Animals)	8.7E-06
LXR/RXR activation	5.5E-05
Epoxysqualene biosynthesis	6.3E-05
LPS/IL-1 mediated inhibition of RXR function	7.8E-05
Fatty acid activation	1.3E-04
Stearate biosynthesis I (Animals)	3.2E-04
Mitochondrial L-carnitine shuttle pathway	3.2E-04
FXR/RXR activation	5.4E-04

Table 7. Relative Expression of Lipogenic Genes in LIM1215(A) Xenograft Tumors.

Gene	Relative expression per treatment group versus vehicle control, mean (SD)				
	P	**B**	**PB**	**BP**	**BB**
FASN	0.952 (0.284)	1.328 (0.436)	1.072 (0.305)	0.762 (0.369)	2.008 (0.311)
MVD	0.661 (0.301)	1.396 (0.249)	0.696 (0.060)	0.679 (0.338)	1.950 (0.459)
LSS	0.820 (0.476)	1.285 (0.234)	0.811 (0.102)	0.751 (0.393)	1.747 (0.227)
HMGCR	0.759 (0.424)	1.303 (0.142)	1.054 (0.165)	0.814 (0.298)	1.796 (0.427)

FASN, fatty acid synthase; HMGCR, HMG-CoA reductase; LSS, lanosterol synthase; MVD, mevalonate disphosphate decarboxylase; P, panitumumab; B, bevacizumab;
PB, panitumumab-bevacizumab; BP, bevacizumab-panitumumab;
BB,bevacizumab-bevacizumab

Table 8. Enrichment Analysis in LIM1215(A) Xenografts Treated with (A) Panitumumab -Bevacizumab. (B) Bevacizumab-Panitumumab. (C) Panitumumab (all Canonical Pathways, $p < 0.001$)

Ingenuity canonical pathways altered versus vehicle control	p-value
A. Panitumumab-bevacizumab (PB)	
Interferon signaling	8.9E-07
UVA-Induced MAPK signaling	2.6E-04
Death receptor signaling	4.6E-04
Role of JAK family kinases in IL-6-type cytokine signaling	7.9E-04
B. Bevacizumab-panitumumab (BP)	
Role of NFAT in cardiac hypertrophy	9.8E-04
C. Panitumumab	
Superpathway of cholesterol biosynthesis	9.1E-05
Regulation of actin-based motility by Rho	1.9E-04
P53 signaling	2.3E-04
Phospholipase C signaling	3.0E-04
Mevalonate pathway I	3.2E-04
Protein kinase A signaling	5.4E-04
D-myo-inositol (1,4,5)-triphosphate biosynthesis	7.4E-04

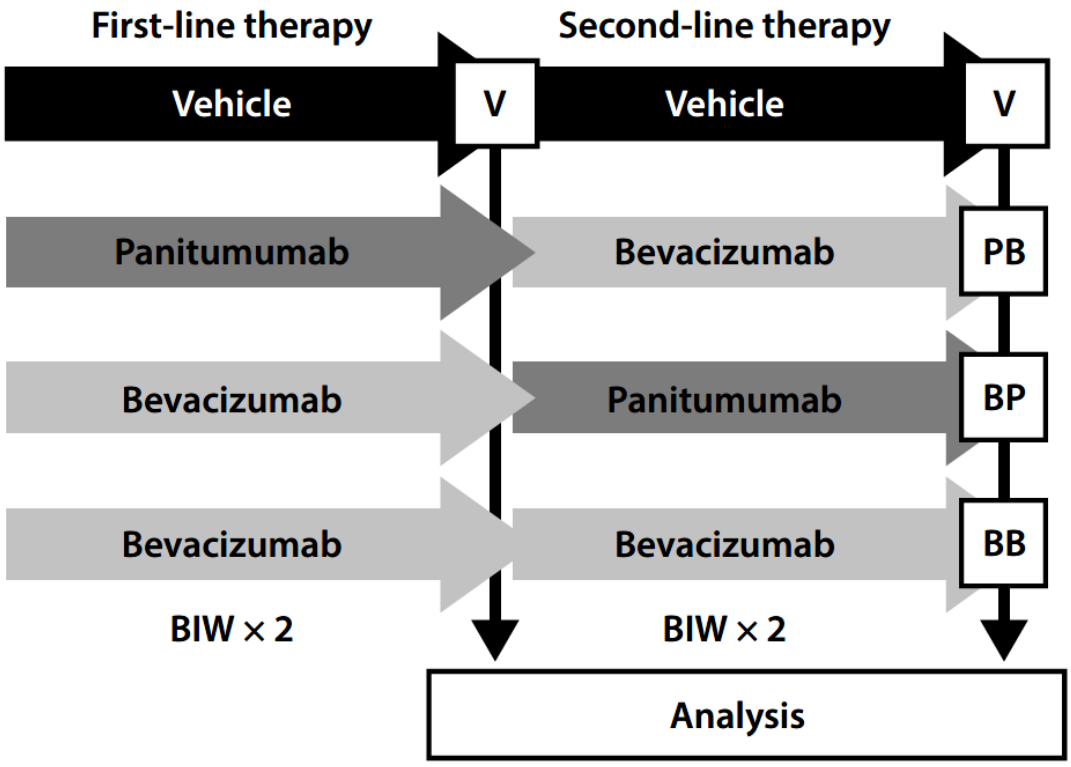

Figure 17. Sequential treatment study design. BIW x 2, twice-weekly for two weeks; V, vehicle control.

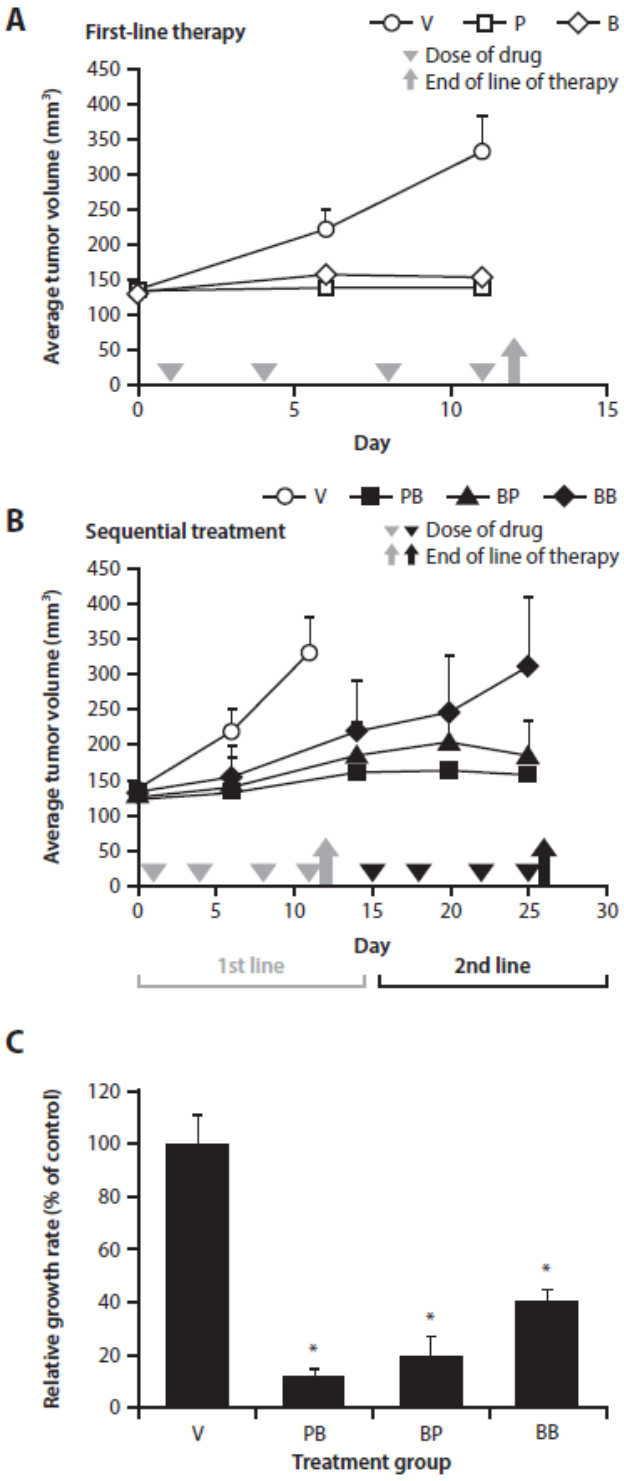

Figure 18. Antitumor effect in LIM1215(A) xenografts by treatment received. Response in the xenograft models was assessed by average tumor volume (A, B) and relative growth rate (C). Arrowheads indicate dosing. Arrows indicate sample harvesting. Data represent mean ± SE. ($n = 3$–7. * $p < 0.05$). B, bevacizumab; P, panitumumab; V, vehicle control.

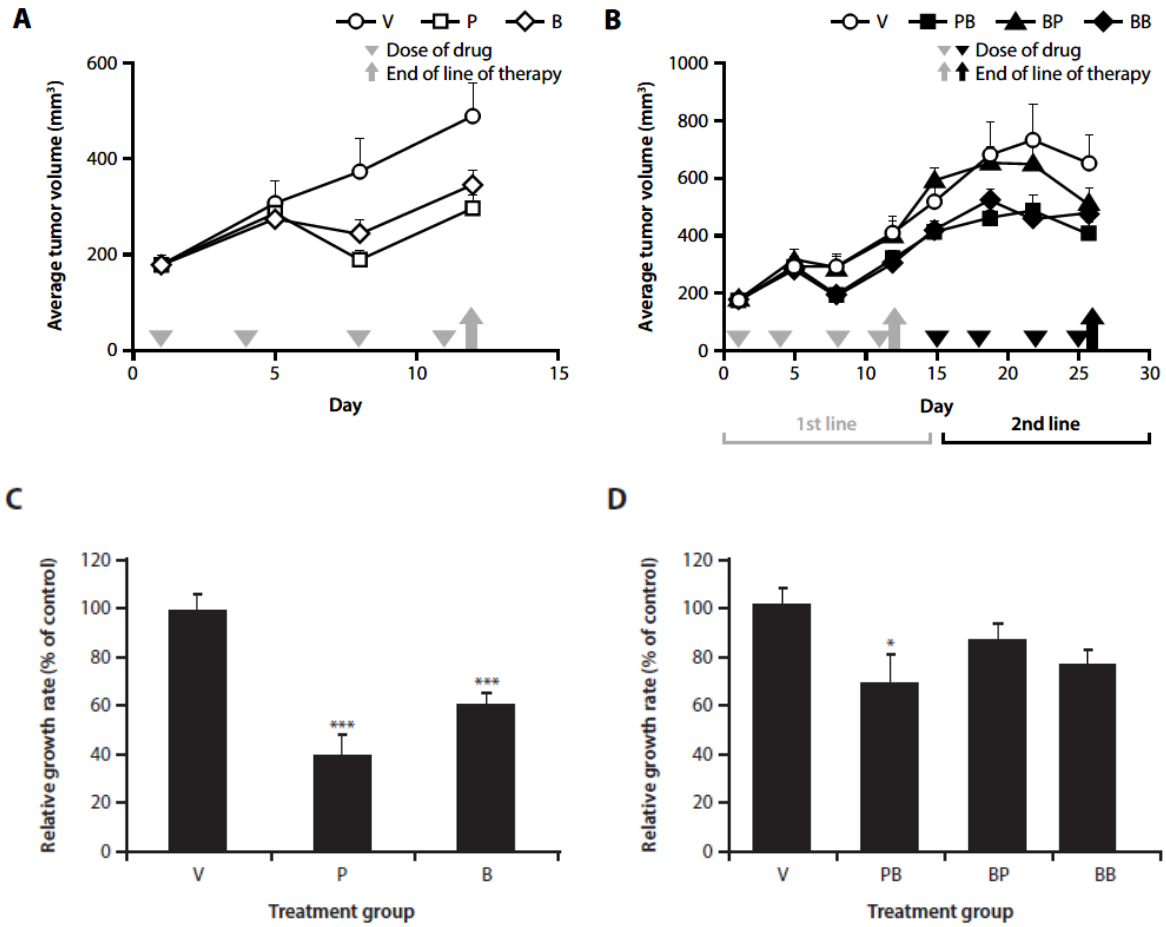

Figure 19. Antitumor effect in LIM1215(B) xenografts by treatment received. Response in the xenograft models was assessed by average tumor volume (A, B) and by relative growth rate (C, D). Arrowheads indicate dosing. Arrows indicate sample harvesting. Data represent mean ± SE. (n = 8). * $p < 0.05$, *** $p < 0.001$. B, bevacizumab; P, panitumumab; V, vehicle control.

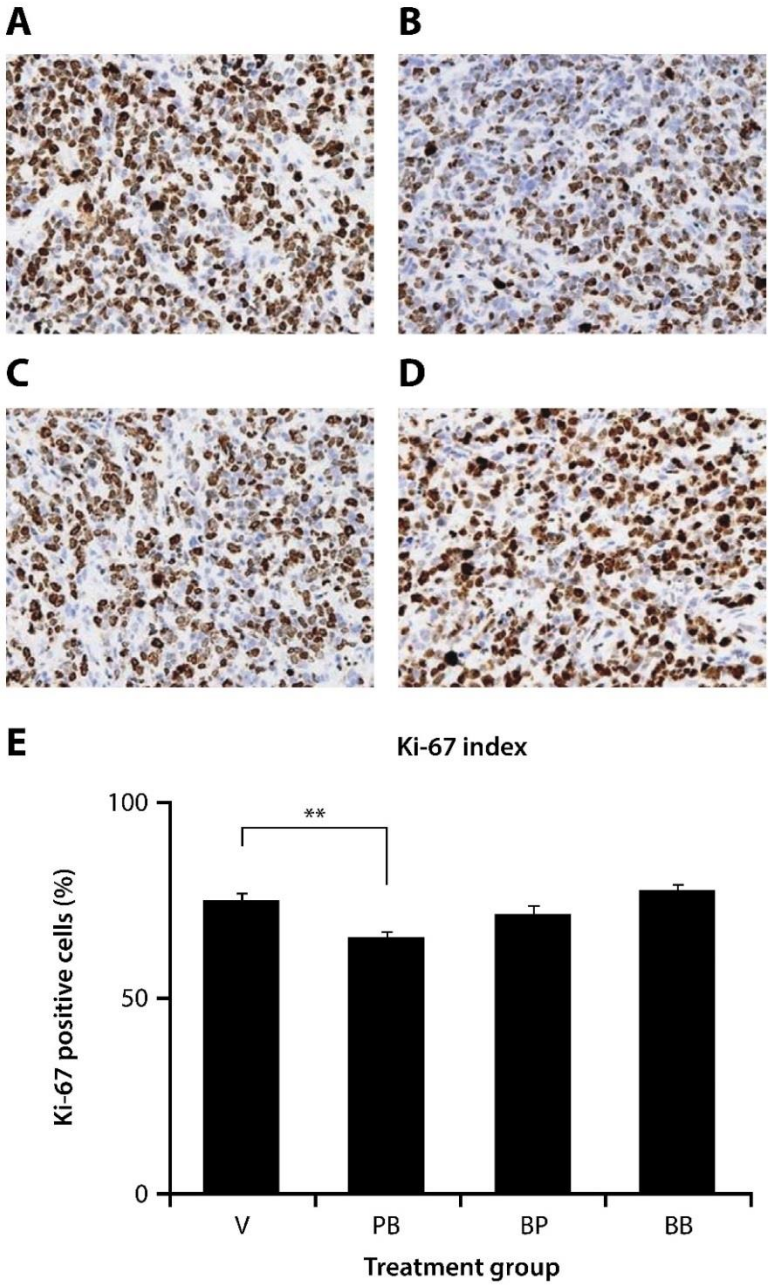

Figure 20. Outcome of immunohistochemistry for Ki-67 in LIM1215(B) xenograft sections. Proliferative rate of LIM1215 cells treated with the vehicle control (A), panitumumab-bevacizumab (B), bevacizumab-panitumumab (C) and bevacizumab-bevacizumab (D). Proportion of Ki-67-positive cells in all treatment groups. Sections were IHC stained for Ki-67 (brown) and counterstained with hematoxylin (purple). Representative images of the sections are shown. Data (E) in the graph represent the mean ± SE (n = 6-8). ** $p < 0.01$. B, bevacizumab; P, panitumumab; V, vehicle control.

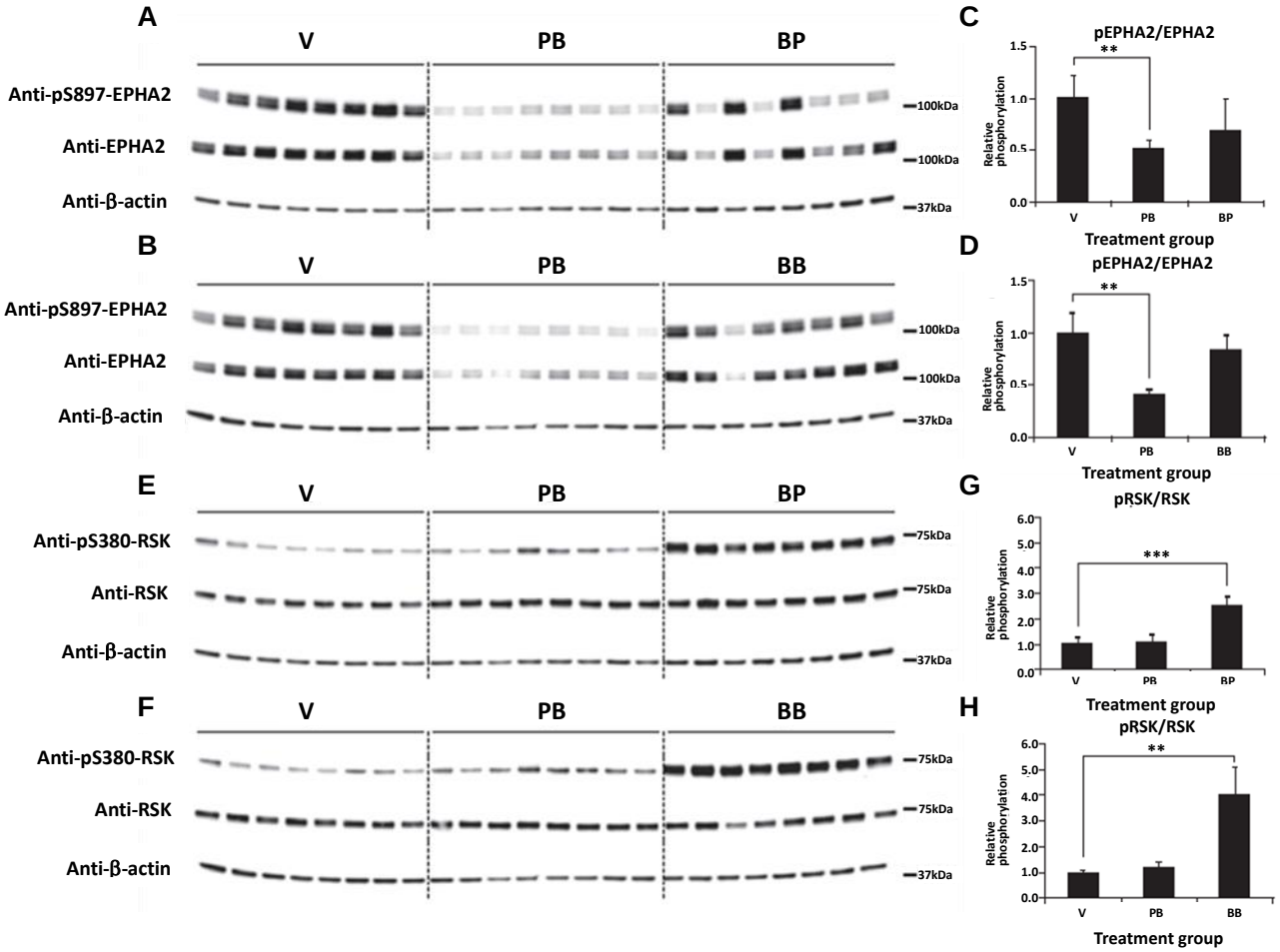

Figure 21. Results of western blotting in LIM1215(B) xenografts. EPHA2 and pEPHA2 (A) with panitumumab-bevacizumab compared with bevacizumab-panitumumab. EPHA2 and pEPHA2 (B) with panitumumab-bevacizumab compared with bevacizumab-bevacizumab. Phosphorylation of EPHA2 for panitumumab-bevacizumab compared with bevacizumab-panitumumab (C) and compared with bevacizumab-bevacizumab (D). RSK and pRSK (E) with panitumumab-bevacizumab compared with bevacizumab-panitumumab and RSK and pRSK (F) with panitumumab-bevacizumab compared with bevacizumab-bevacizumab. Phosphorylation of RSK for panitumumab-bevacizumab compared with bevacizumab-panitumumab (G) and compared with bevacizumab-bevacizumab (H). Data represent mean ± SD (n = 8). ** $p < 0.01$, *** $p < 0.001$. B, bevacizumab; P, panitumumab; V, vehicle control.

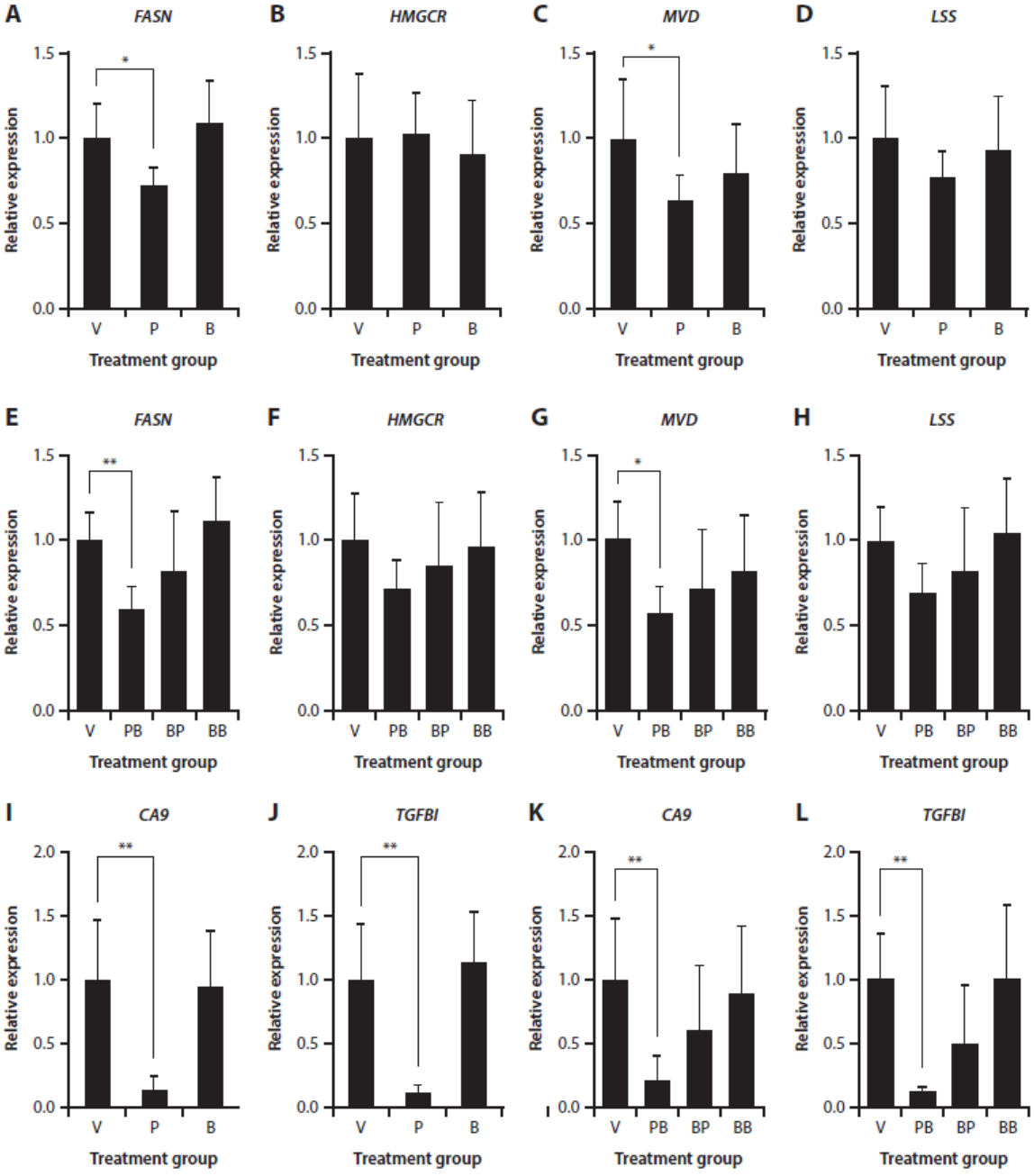

Figure 22. Relative expression of lipogenic (*FASN, HMGCR, MVD, LSS*) and hypoxia-related (*CA9, TGFBI*) genes in LIM1215(B) xenograft tumors. Expression relative to vehicle control with first-line treatment (A-D, I, J) is shown, and with sequential treatment (E-H, K, L). Data represent mean ± SD ($n = 8$). * $p < 0.05$, ** $p < 0.01$.
B, bevacizumab; P, panitumumab; V, vehicle control.

General Discussion

In the first chapter of this thesis, I demonstrated that the combination of panitumumab and TAS-102 had a more robust antitumor effect than either single agent. In addition, I found that TAS-102 induced serine/threonine phosphorylation of the EGFR. Interestingly, I also showed that panitumumab suppressed the activation of ERK/AKT/STAT3, a malignant cancer determinant induced by TAS-102. In the second chapter of this dissertation, I established that the sequential administration of PB exhibited a more robust inhibition of tumor growth than BP administration. In addition, I found that administration of PB significantly reduced EPHA2 phosphorylation as well as genes involved in lipogenesis and hypoxia, which are also malignant cancer determinants. These preclinical findings may provide a compelling rationale for evaluating the efficacy of a combination of panitumumab and TAS-102 for the treatment of CRC. In addition, these studies reveal that the administration of PB may be useful for treating CRC.

These studies were conducted with xenograft models of human CRC. There are several limitations associated with the use of xenograft models of human cancers, including the inability of these models to recapitulate the complexity of human cancer[115]. In particular, heterotopic xenograft models, as used in the current study, cannot reproduce the complex tumor-stroma interactions of human autochthonous colorectal carcinoma. Furthermore, xenograft tumors lack the heterogeneity

of human tumors due to their construction from standardized cell lines. In addition, tumor interactions with the immune system are compromised in SCID mice. There are also key experimental design factors that differ between studies of xenograft models and cancer in the clinical setting, including the time scales over which the tumor develops and is treated. In the first chapter, my results does not indicate whether the combination of panitumumab and TAS-102 continue to induce tumor regression. In the second chapter, xenograft models in the current study did not become resistant to first-line therapies as would be expected in the clinic; the two-week experimental period was not sufficient to show resistance. Also, other potential factors contributing to anti-EGFR antibody therapy resistance, such as protein levels of VEGF ligands and vascular endothelial growth factor receptor (VEGFR)[86,90,91], were not monitored in the current study; VEGFA mRNA did not change in my transcriptome data, and phosphoproteomic analysis could not detect VEGF-A and VEGFR peptides. Accordingly, further analysis of current clinical trials (APOLLON study and PARADIGM study) is necessary to confirm the differences between human and xenograft models.

Meanwhile, it is crucial that non-clinical data verify the importance of a drug treatment and potential of a drug treatment efficacy before clinical trials. Since clinical samples are difficult to obtain, and even if obtained, are difficult to analyze due to their heterogeneity and stability, it is

important to obtain the data with non-clinical samples because they are easy to obtain and analyze. Since several papers often suggest many hypotheses to explain their clinical trial data, evidence that has been confirmed by non-clinical data are required.

As described above, the differences between clinical and non-clinical data are crucial for evaluating the efficacy of antibody therapy and/or chemotherapy for the treatment of CRC. However, solving the question of which drug to use and in what order will be a significant advance in treating CRC. Since soaring drug costs have become a social issue, considering the combination and sequential order of existing drugs is very meaningful from the viewpoint of reducing medical costs. In the future, research on existing drugs is expected to increase.

Acknowledgements

I am deeply grateful to Professors Kazuichi Sakamoto, Chikafumi Chiba, Hidekazu Kuwayama and Yuji Inagaki, University of Tsukuba, for guiding my work and valuable discussions through my doctoral program. I would like to thank Toshiya Tamura, Yoshihiko Satoh, Masamitsu Gotou, Hiroshi Sawada, Shunsuke Ebara, Kazunori Yamanaka, Kazuhide Nakamura, Akio, Mizutani, Tadahiro Nambu, Yasuko Tsuchiya, Asako Tagashira, Saomi Murai, Ryo Fukuda and Kotaro Yokoyama for technical assistance and Kazunori Shibuya, Jumpei Soeda, Hiroya Taniguchi, Yoji Sagiya, Yukiko Sakakibara, Ikuo Mori, Yukiko Hikichi, Hideo Baba, Atsushi Kiba, Toshiyuki Nomura, and Hiroshi Miyake for their guidance and support during the course of this work. Assistance for this manuscript publication was provided by Miki Kikko, Yumi Oomuku and Tsuyoshi Osaka.

References

1 Ferlay, J. *et al.* Estimating the global cancer incidence and mortality in 2018: GLOBOCAN sources and methods. *International journal of cancer* **144**, 1941-1953, doi:10.1002/ijc.31937 (2019).

2 Araghi, M. *et al.* Global trends in colorectal cancer mortality: projections to the year 2035. *International journal of cancer* **144**, 2992-3000, doi:10.1002/ijc.32055 (2019).

3 Van Cutsem, E., Cervantes, A., Nordlinger, B. & Arnold, D. Metastatic colorectal cancer: ESMO Clinical Practice Guidelines for diagnosis, treatment and follow-up. *Annals of oncology : official journal of the European Society for Medical Oncology* **25 Suppl 3**, iii1-9, doi:10.1093/annonc/mdu260 (2014).

4 Jonker, D. J. *et al.* Cetuximab for the treatment of colorectal cancer. *The New England journal of medicine* **357**, 2040-2048, doi:10.1056/NEJMoa071834 (2007).

5 Van Cutsem, E. *et al.* Open-label phase III trial of panitumumab plus best supportive care compared with best supportive care alone in patients with chemotherapy-refractory metastatic colorectal cancer. *Journal of clinical oncology : official journal of the American Society of Clinical Oncology* **25**, 1658-1664, doi:10.1200/jco.2006.08.1620 (2007).

6 Fakih, M. G. Metastatic colorectal cancer: current state and future directions. *Journal of clinical oncology : official journal of the American Society of Clinical Oncology* **33**, 1809-1824, doi:10.1200/jco.2014.59.7633 (2015).

7 Bennouna, J. *et al.* Continuation of bevacizumab after first progression in metastatic colorectal cancer (ML18147): a randomised phase 3 trial. *The Lancet. Oncology* **14**, 29-37, doi:10.1016/s1470-2045(12)70477-1 (2013).

8 Bokemeyer, C. *et al.* Addition of cetuximab to chemotherapy as first-line treatment for KRAS wild-type metastatic colorectal cancer: pooled analysis of the CRYSTAL and OPUS randomised clinical trials. *European journal of cancer (Oxford, England : 1990)* **48**, 1466-1475, doi:10.1016/j.ejca.2012.02.057 (2012).

9 Cunningham, D. *et al.* Bevacizumab plus capecitabine versus capecitabine alone in elderly patients with previously untreated metastatic colorectal cancer (AVEX): an open-label, randomised phase 3 trial. *The Lancet. Oncology* **14**, 1077-1085, doi:10.1016/s1470-2045(13)70154-2 (2013).

10 Douillard, J. Y. *et al.* Panitumumab-FOLFOX4 treatment and RAS mutations in colorectal cancer. *The New England journal of medicine* **369**, 1023-1034, doi:10.1056/NEJMoa1305275 (2013).

11 Hu, W., Xu, W. S., Liao, X. F. & He, H. J. Bevacizumab in combination with first-line chemotherapy in patients with metastatic colorectal cancer: a meta-analysis. *Minerva chirurgica* **70**, 451-458 (2015).

12 Peeters, M. *et al.* Analysis of KRAS/NRAS Mutations in a Phase III Study of Panitumumab with FOLFIRI Compared with FOLFIRI Alone as Second-line Treatment for Metastatic Colorectal Cancer. *Clinical cancer research : an official journal of the American Association for Cancer Research* **21**, 5469-5479, doi:10.1158/1078-0432.ccr-15-0526 (2015).

13 Yarden, Y. & Sliwkowski, M. X. Untangling the ErbB signalling network. *Nature reviews. Molecular cell biology* **2**, 127-137, doi:10.1038/35052073 (2001).

14 Scaltriti, M. & Baselga, J. The epidermal growth factor receptor pathway: a model for targeted therapy. *Clinical cancer research : an official journal of the American Association for Cancer Research* **12**, 5268-5272, doi:10.1158/1078-0432.ccr-05-1554 (2006).

15 Hynes, N. E. & Lane, H. A. ERBB receptors and cancer: the complexity of targeted inhibitors. *Nature reviews. Cancer* **5**, 341-354, doi:10.1038/nrc1609 (2005).

16 Hamaoka, Y., Negishi, M. & Katoh, H. EphA2 is a key effector of the MEK/ERK/RSK pathway regulating glioblastoma cell proliferation. *Cellular signalling* **28**, 937-945,

doi:10.1016/j.cellsig.2016.04.009 (2016).
17 Kaibori, Y., Saito, Y. & Nakayama, Y. EphA2 phosphorylation at Ser897 by the Cdk1/MEK/ERK/RSK pathway regulates M-phase progression via maintenance of cortical rigidity. *FASEB journal : official publication of the Federation of American Societies for Experimental Biology* **33**, 5334-5349, doi:10.1096/fj.201801519RR (2019).
18 Herath, N. I. *et al.* Complex expression patterns of Eph receptor tyrosine kinases and their ephrin ligands in colorectal carcinogenesis. *European journal of cancer (Oxford, England : 1990)* **48**, 753-762, doi:10.1016/j.ejca.2011.07.003 (2012).
19 Dunne, P. D. *et al.* EphA2 Expression Is a Key Driver of Migration and Invasion and a Poor Prognostic Marker in Colorectal Cancer. *Clinical cancer research : an official journal of the American Association for Cancer Research* **22**, 230-242, doi:10.1158/1078-0432.ccr-15-0603 (2016).
20 Zhou, Y. *et al.* Crucial roles of RSK in cell motility by catalysing serine phosphorylation of EphA2. *Nature communications* **6**, 7679, doi:10.1038/ncomms8679 (2015).
21 Miao, H. *et al.* EphA2 mediates ligand-dependent inhibition and ligand-independent promotion of cell migration and invasion via a reciprocal regulatory loop with Akt. *Cancer cell* **16**, 9-20, doi:10.1016/j.ccr.2009.04.009 (2009).
22 Spano, J. P. *et al.* Impact of EGFR expression on colorectal cancer patient prognosis and survival. *Annals of oncology : official journal of the European Society for Medical Oncology* **16**, 102-108, doi:10.1093/annonc/mdi006 (2005).
23 Mizukami, T., Izawa, N., Nakajima, T. E. & Sunakawa, Y. Targeting EGFR and RAS/RAF Signaling in the Treatment of Metastatic Colorectal Cancer: From Current Treatment Strategies to Future Perspectives. *Drugs* **79**, 633-645, doi:10.1007/s40265-019-01113-0 (2019).
24 Saif, M. W., Peccerillo, J. & Potter, V. Successful re-challenge with panitumumab in patients who developed hypersensitivity reactions to cetuximab: report of three cases and review of literature. *Cancer chemotherapy and pharmacology* **63**, 1017-1022, doi:10.1007/s00280-008-0831-6 (2009).
25 Kang, S. P. & Saif, M. W. Infusion-related and hypersensitivity reactions of monoclonal antibodies used to treat colorectal cancer--identification, prevention, and management. *The journal of supportive oncology* **5**, 451-457 (2007).
26 Karapetis, C. S. *et al.* K-ras mutations and benefit from cetuximab in advanced colorectal cancer. *The New England journal of medicine* **359**, 1757-1765, doi:10.1056/NEJMoa0804385 (2008).
27 Amado, R. G. *et al.* Wild-type KRAS is required for panitumumab efficacy in patients with metastatic colorectal cancer. *Journal of clinical oncology : official journal of the American Society of Clinical Oncology* **26**, 1626-1634, doi:10.1200/jco.2007.14.7116 (2008).
28 Siena, S., Sartore-Bianchi, A., Di Nicolantonio, F., Balfour, J. & Bardelli, A. Biomarkers predicting clinical outcome of epidermal growth factor receptor-targeted therapy in metastatic colorectal cancer. *Journal of the National Cancer Institute* **101**, 1308-1324, doi:10.1093/jnci/djp280 (2009).
29 Heinemann, V. *et al.* A study-level meta-analysis of efficacy data from head-to-head first-line trials of epidermal growth factor receptor inhibitors versus bevacizumab in patients with RAS wild-type metastatic colorectal cancer. *Eur J Cancer* **67**, 11-20, doi:10.1016/j.ejca.2016.07.019 (2016).
30 Salvatore, L. *et al.* TAS-102 for the treatment of metastatic colorectal cancer. *Expert review of anticancer therapy* **15**, 1283-1292, doi:10.1586/14737140.2015.1105746 (2015).
31 Peters, G. J. Therapeutic potential of TAS-102 in the treatment of gastrointestinal malignancies. *Therapeutic advances in medical oncology* **7**, 340-356, doi:10.1177/1758834015603313 (2015).

32 Fukushima, M. *et al.* Structure and activity of specific inhibitors of thymidine phosphorylase to potentiate the function of antitumor 2'-deoxyribonucleosides. *Biochemical pharmacology* **59**, 1227-1236 (2000).
33 Temmink, O. H., Emura, T., de Bruin, M., Fukushima, M. & Peters, G. J. Therapeutic potential of the dual-targeted TAS-102 formulation in the treatment of gastrointestinal malignancies. *Cancer science* **98**, 779-789, doi:10.1111/j.1349-7006.2007.00477.x (2007).
34 Reyes, P. & Heidelberger, C. Fluorinated pyrimidines. XXVI. Mammalian thymidylate synthetase: its mechanism of action and inhibition by fluorinated nucleotides. *Molecular pharmacology* **1**, 14-30 (1965).
35 Santi, D. V. & Sakai, T. T. Thymidylate synthetase. Model studies of inhibition by 5-trifluoromethyl-2'-deoxyuridylic acid. *Biochemistry* **10**, 3598-3607 (1971).
36 Eckstein, J. W., Foster, P. G., Finer-Moore, J., Wataya, Y. & Santi, D. V. Mechanism-based inhibition of thymidylate synthase by 5-(trifluoromethyl)-2'-deoxyuridine 5'-monophosphate. *Biochemistry* **33**, 15086-15094 (1994).
37 Tanaka, N. *et al.* Repeated oral dosing of TAS-102 confers high trifluridine incorporation into DNA and sustained antitumor activity in mouse models. *Oncology reports* **32**, 2319-2326, doi:10.3892/or.2014.3487 (2014).
38 Van Triest, B. & Peters, G. J. Thymidylate synthase: a target for combination therapy and determinant of chemotherapeutic response in colorectal cancer. *Oncology* **57**, 179-194, doi:10.1159/000012030 (1999).
39 Temmink, O. H., Comijn, E. M., Fukushima, M. & Peters, G. J. Intracellular thymidylate synthase inhibition by trifluorothymidine in FM3A cells. *Nucleosides, nucleotides & nucleic acids* **23**, 1491-1494, doi:10.1081/ncn-200027707 (2004).
40 Suzuki, N., Emura, T. & Fukushima, M. Mode of action of trifluorothymidine (TFT) against DNA replication and repair enzymes. *International journal of oncology* **39**, 263-270, doi:10.3892/ijo.2011.1003 (2011).
41 Matsuoka, K. *et al.* Trifluridine Induces p53-Dependent Sustained G2 Phase Arrest with Its Massive Misincorporation into DNA and Few DNA Strand Breaks. *Molecular cancer therapeutics* **14**, 1004-1013, doi:10.1158/1535-7163.mct-14-0236 (2015).
42 Emura, T., Murakami, Y., Nakagawa, F., Fukushima, M. & Kitazato, K. A novel antimetabolite, TAS-102 retains its effect on FU-related resistant cancer cells. *International journal of molecular medicine* **13**, 545-549 (2004).
43 Emura, T., Suzuki, N., Yamaguchi, M., Ohshimo, H. & Fukushima, M. A novel combination antimetabolite, TAS-102, exhibits antitumor activity in FU-resistant human cancer cells through a mechanism involving FTD incorporation in DNA. *International journal of oncology* **25**, 571-578 (2004).
44 van der Velden, D. L., Opdam, F. L. & Voest, E. E. TAS-102 for Treatment of Advanced Colorectal Cancers That Are No Longer Responding to Other Therapies. *Clinical cancer research : an official journal of the American Association for Cancer Research* **22**, 2835-2839, doi:10.1158/1078-0432.ccr-15-2783 (2016).
45 Mayer, R. J. *et al.* Randomized trial of TAS-102 for refractory metastatic colorectal cancer. *N Engl J Med* **372**, 1909-1919, doi:10.1056/NEJMoa1414325 (2015).
46 Tsukihara, H. *et al.* Efficacy of combination chemotherapy using a novel oral chemotherapeutic agent, TAS-102, together with bevacizumab, cetuximab, or panitumumab on human colorectal cancer xenografts. *Oncology reports* **33**, 2135-2142, doi:10.3892/or.2015.3876 (2015).
47 Franken, N. A., Rodermond, H. M., Stap, J., Haveman, J. & van Bree, C. Clonogenic assay of cells in vitro. *Nature protocols* **1**, 2315-2319, doi:10.1038/nprot.2006.339 (2006).
48 Garcia, K. *et al.* Nedd8-activating enzyme inhibitor MLN4924 provides synergy with mitomycin C through interactions with ATR, BRCA1/BRCA2, and chromatin

dynamics pathways. *Molecular cancer therapeutics* **13**, 1625-1635, doi:10.1158/1535-7163.mct-13-0634 (2014).
49 Minto, C. F. *et al.* Response surface model for anesthetic drug interactions. *Anesthesiology* **92**, 1603-1616 (2000).
50 Berenbaum, M. C. The expected effect of a combination of agents: the general solution. *Journal of theoretical biology* **114**, 413-431 (1985).
51 Chou, T. C. & Talalay, P. Quantitative analysis of dose-effect relationships: the combined effects of multiple drugs or enzyme inhibitors. *Advances in enzyme regulation* **22**, 27-55 (1984).
52 Peterson, J. J. & Novick, S. J. Nonlinear blending: a useful general concept for the assessment of combination drug synergy. *Journal of receptor and signal transduction research* **27**, 125-146, doi:10.1080/10799890701417576 (2007).
53 Kitao, H. *et al.* The antibodies against 5-bromo-2'-deoxyuridine specifically recognize trifluridine incorporated into DNA. *Scientific reports* **6**, 25286, doi:10.1038/srep25286 (2016).
54 Horn, H. *et al.* KinomeXplorer: an integrated platform for kinome biology studies. *Nature methods* **11**, 603-604, doi:10.1038/nmeth.2968 (2014).
55 Shannon, P. *et al.* Cytoscape: a software environment for integrated models of biomolecular interaction networks. *Genome research* **13**, 2498-2504, doi:10.1101/gr.1239303 (2003).
56 Huang da, W., Sherman, B. T. & Lempicki, R. A. Bioinformatics enrichment tools: paths toward the comprehensive functional analysis of large gene lists. *Nucleic acids research* **37**, 1-13, doi:10.1093/nar/gkn923 (2009).
57 Huang da, W., Sherman, B. T. & Lempicki, R. A. Systematic and integrative analysis of large gene lists using DAVID bioinformatics resources. *Nature protocols* **4**, 44-57, doi:10.1038/nprot.2008.211 (2009).
58 Bijnsdorp, I. V. *et al.* Molecular mechanism underlying the synergistic interaction between trifluorothymidine and the epidermal growth factor receptor inhibitor erlotinib in human colorectal cancer cell lines. *Cancer science* **101**, 440-447, doi:10.1111/j.1349-7006.2009.01375.x (2010).
59 Chu, E. *et al.* Autoregulation of human thymidylate synthase messenger RNA translation by thymidylate synthase. *Proceedings of the National Academy of Sciences of the United States of America* **88**, 8977-8981 (1991).
60 Nukatsuka, M. *et al.* Efficacy of combination chemotherapy using a novel oral chemotherapeutic agent, TAS-102, with irinotecan hydrochloride on human colorectal and gastric cancer xenografts. *Anticancer research* **35**, 1437-1445 (2015).
61 Temmink, O. H. *et al.* Mechanism of trifluorothymidine potentiation of oxaliplatin-induced cytotoxicity to colorectal cancer cells. *British journal of cancer* **96**, 231-240, doi:10.1038/sj.bjc.6603549 (2007).
62 McCubrey, J. A. *et al.* Therapeutic resistance resulting from mutations in Raf/MEK/ERK and PI3K/PTEN/Akt/mTOR signaling pathways. *Journal of cellular physiology* **226**, 2762-2781, doi:10.1002/jcp.22647 (2011).
63 Liu, Q., Turner, K. M., Alfred Yung, W. K., Chen, K. & Zhang, W. Role of AKT signaling in DNA repair and clinical response to cancer therapy. *Neuro-oncology* **16**, 1313-1323, doi:10.1093/neuonc/nou058 (2014).
64 Winograd-Katz, S. E. & Levitzki, A. Cisplatin induces PKB/Akt activation and p38(MAPK) phosphorylation of the EGF receptor. *Oncogene* **25**, 7381-7390, doi:10.1038/sj.onc.1209737 (2006).
65 Mabuchi, S. *et al.* Inhibition of phosphorylation of BAD and Raf-1 by Akt sensitizes human ovarian cancer cells to paclitaxel. *The Journal of biological chemistry* **277**, 33490-33500, doi:10.1074/jbc.M204042200 (2002).
66 Taylor, J. R. *et al.* Cooperative effects of Akt-1 and Raf-1 on the induction of cellular senescence in doxorubicin or tamoxifen treated breast cancer cells. *Oncotarget* **2**,

610-626, doi:10.18632/oncotarget.315 (2011).
67 Poli, V. & Camporeale, A. STAT3-Mediated Metabolic Reprograming in Cellular Transformation and Implications for Drug Resistance. *Frontiers in oncology* **5**, 121, doi:10.3389/fonc.2015.00121 (2015).
68 Li, X., Huang, Y., Jiang, J. & Frank, S. J. ERK-dependent threonine phosphorylation of EGF receptor modulates receptor downregulation and signaling. *Cellular signalling* **20**, 2145-2155, doi:10.1016/j.cellsig.2008.08.006 (2008).
69 Takishima, K., Griswold-Prenner, I., Ingebritsen, T. & Rosner, M. R. Epidermal growth factor (EGF) receptor T669 peptide kinase from 3T3-L1 cells is an EGF-stimulated "MAP" kinase. *Proceedings of the National Academy of Sciences of the United States of America* **88**, 2520-2524, doi:10.1073/pnas.88.6.2520 (1991).
70 Northwood, I. C., Gonzalez, F. A., Wartmann, M., Raden, D. L. & Davis, R. J. Isolation and characterization of two growth factor-stimulated protein kinases that phosphorylate the epidermal growth factor receptor at threonine 669. *The Journal of biological chemistry* **266**, 15266-15276 (1991).
71 Nishimura, M. *et al.* TAK1-mediated serine/threonine phosphorylation of epidermal growth factor receptor via p38/extracellular signal-regulated kinase: NF-{kappa}B-independent survival pathways in tumor necrosis factor alpha signaling. *Molecular and cellular biology* **29**, 5529-5539, doi:10.1128/mcb.00375-09 (2009).
72 Zhao, B. *et al.* Mechanisms of resistance to anti-EGFR therapy in colorectal cancer. *Oncotarget* **8**, 3980-4000, doi:10.18632/oncotarget.14012 (2017).
73 Therkildsen, C., Bergmann, T. K., Henrichsen-Schnack, T., Ladelund, S. & Nilbert, M. The predictive value of KRAS, NRAS, BRAF, PIK3CA and PTEN for anti-EGFR treatment in metastatic colorectal cancer: A systematic review and meta-analysis. *Acta oncologica (Stockholm, Sweden)* **53**, 852-864, doi:10.3109/0284186x.2014.895036 (2014).
74 Van Cutsem, E. *et al.* Fluorouracil, leucovorin, and irinotecan plus cetuximab treatment and RAS mutations in colorectal cancer. *Journal of clinical oncology : official journal of the American Society of Clinical Oncology* **33**, 692-700, doi:10.1200/jco.2014.59.4812 (2015).
75 Stintzing, S. *et al.* FOLFIRI plus cetuximab versus FOLFIRI plus bevacizumab for metastatic colorectal cancer (FIRE-3): a post-hoc analysis of tumour dynamics in the final RAS wild-type subgroup of this randomised open-label phase 3 trial. *The Lancet. Oncology* **17**, 1426-1434, doi:10.1016/s1470-2045(16)30269-8 (2016).
76 Cox, A. D., Fesik, S. W., Kimmelman, A. C., Luo, J. & Der, C. J. Drugging the undruggable RAS: Mission possible? *Nature reviews. Drug discovery* **13**, 828-851, doi:10.1038/nrd4389 (2014).
77 Peeters, M. *et al.* Prevalence of RAS mutations and individual variation patterns among patients with metastatic colorectal cancer: A pooled analysis of randomised controlled trials. *European journal of cancer (Oxford, England : 1990)* **51**, 1704-1713, doi:10.1016/j.ejca.2015.05.017 (2015).
78 Hanahan, D. & Weinberg, R. A. Hallmarks of cancer: the next generation. *Cell* **144**, 646-674, doi:10.1016/j.cell.2011.02.013 (2011).
79 Goel, S., Huang, J. & Klampfer, L. K-Ras, intestinal homeostasis and colon cancer. *Current clinical pharmacology* **10**, 73-81 (2015).
80 Modest, D. P. *et al.* Impact of Subsequent Therapies on Outcome of the FIRE-3/AIO KRK0306 Trial: First-Line Therapy With FOLFIRI Plus Cetuximab or Bevacizumab in Patients With KRAS Wild-Type Tumors in Metastatic Colorectal Cancer. *Journal of clinical oncology : official journal of the American Society of Clinical Oncology* **33**, 3718-3726, doi:10.1200/jco.2015.61.2887 (2015).
81 Zaniboni, A. & Formica, V. The Best. First. Anti-EGFR before anti-VEGF, in the first-line treatment of RAS wild-type metastatic colorectal cancer: from bench to bedside. *Cancer chemotherapy and pharmacology* **78**, 233-244,

doi:10.1007/s00280-016-3032-8 (2016).
82 Wainberg, Z. A. & Drakaki, A. The importance of optimal drug sequencing in metastatic colorectal cancer: biological rationales for the observed survival benefit conferred by first-line treatment with EGFR inhibitors. *Expert opinion on biological therapy* **15**, 1205-1220, doi:10.1517/14712598.2015.1050375 (2015).
83 Peeters, M. *et al.* Exploratory pooled analysis evaluating the effect of sequence of biological therapies on overall survival in patients with RAS wild-type metastatic colorectal carcinoma. *ESMO open* **3**, e000297, doi:10.1136/esmoopen-2017-000297 (2018).
84 Lam, K. O., Lee, V. H., Liu, R. K., Leung, T. W. & Kwong, D. L. Bevacizumab-containing regimens after cetuximab failure in Kras wild-type metastatic colorectal carcinoma. *Oncology letters* **5**, 637-640, doi:10.3892/ol.2012.1045 (2013).
85 Hasegawa, H. *et al.* Efficacy of Second-Line Bevacizumab-Containing Chemotherapy for Patients with Metastatic Colorectal Cancer following First-Line Treatment with an Anti-Epidermal Growth Factor Receptor Antibody. *Oncology* **92**, 205-212, doi:10.1159/000453336 (2017).
86 Derangere, V. *et al.* Does bevacizumab impact anti-EGFR therapy efficacy in metastatic colorectal cancer? *Oncotarget* **7**, 9309-9321, doi:10.18632/oncotarget.7008 (2016).
87 Norguet, E. *et al.* Cetuximab after bevacizumab in metastatic colorectal cancer: is it the best sequence? *Digestive and liver disease : official journal of the Italian Society of Gastroenterology and the Italian Association for the Study of the Liver* **43**, 917-919, doi:10.1016/j.dld.2011.06.002 (2011).
88 Sato, Y., Matsusaka, S., Suenaga, M., Shinozaki, E. & Mizunuma, N. Cetuximab could be more effective without prior bevacizumab treatment in metastatic colorectal cancer patients. *OncoTargets and therapy* **8**, 3329-3336, doi:10.2147/ott.s89241 (2015).
89 Taniguchi, H. *et al.* A short interval between bevacizumab and anti-epithelial growth factor receptor therapy interferes with efficacy of subsequent anti-EGFR therapy for refractory colorectal cancer. *Japanese journal of clinical oncology* **46**, 228-233, doi:10.1093/jjco/hyv193 (2016).
90 Baba, H. *et al.* Changes in expression levels of ERCC1, DPYD, and VEGFA mRNA after first-line chemotherapy of metastatic colorectal cancer: results of a multicenter study. *Oncotarget* **6**, 34004-34013, doi:10.18632/oncotarget.5227 (2015).
91 Viloria-Petit, A. *et al.* Acquired resistance to the antitumor effect of epidermal growth factor receptor-blocking antibodies in vivo: a role for altered tumor angiogenesis. *Cancer research* **61**, 5090-5101 (2001).
92 Greening, D. W. *et al.* Molecular profiling of cetuximab and bevacizumab treatment of colorectal tumours reveals perturbations in metabolic and hypoxic response pathways. *Oncotarget* **6**, 38166-38180, doi:10.18632/oncotarget.6241 (2015).
93 Wisniewski, J. R., Zougman, A., Nagaraj, N. & Mann, M. Universal sample preparation method for proteome analysis. *Nature methods* **6**, 359-362, doi:10.1038/nmeth.1322 (2009).
94 Graves, P. R. *et al.* Ionizing radiation induces EphA2 S897 phosphorylation in a MEK/ERK/RSK-dependent manner. *International journal of radiation biology* **93**, 929-936, doi:10.1080/09553002.2017.1355580 (2017).
95 Heskamp, S. *et al.* Bevacizumab reduces tumor targeting of antiepidermal growth factor and anti-insulin-like growth factor 1 receptor antibodies. *International journal of cancer* **133**, 307-314, doi:10.1002/ijc.28046 (2013).
96 Macrae, M. *et al.* A conditional feedback loop regulates Ras activity through EphA2. *Cancer cell* **8**, 111-118, doi:10.1016/j.ccr.2005.07.005 (2005).
97 Pratt, R. L. & Kinch, M. S. Ligand binding up-regulates EphA2 messenger RNA through the mitogen-activated protein/extracellular signal-regulated kinase pathway.

Molecular cancer research : MCR **1**, 1070-1076 (2003).

98 Cardone, C. P., MC. Moreno-Viedma, V. Martini, G. Vitiello, P. Ciardiello, D. Sforza, V. Troiani, T. Napolitano, S. Vitale, P. Zanaletti, N. Rachiglio, AM. Rizzi, D. Maiello, E. Narmanno, N. Sibilia, M. Ciardeiello, F. Martinelli, E. EphA2 expression is a predictive biomarker of poorer activity and efficacy of FOLFIRI + cetuximab in RAS WT metastatis colorectal cancer (mCRC) patients (pts) in the CAPRI-GOIM trial. *Ann Oncol* **28**, abst 1637P (2017).

99 De Robertis, M. *et al.* Dysregulation of EGFR Pathway in EphA2 Cell Subpopulation Significantly Associates with Poor Prognosis in Colorectal Cancer. *Clinical cancer research : an official journal of the American Association for Cancer Research* **23**, 159-170, doi:10.1158/1078-0432.ccr-16-0709 (2017).

100 Barquilla, A. *et al.* Protein kinase A can block EphA2 receptor-mediated cell repulsion by increasing EphA2 S897 phosphorylation. *Molecular biology of the cell* **27**, 2757-2770, doi:10.1091/mbc.E16-01-0048 (2016).

101 Selvakumaran, M., Yao, K. S., Feldman, M. D. & O'Dwyer, P. J. Antitumor effect of the angiogenesis inhibitor bevacizumab is dependent on susceptibility of tumors to hypoxia-induced apoptosis. *Biochemical pharmacology* **75**, 627-638, doi:10.1016/j.bcp.2007.09.029 (2008).

102 Lucien, F., Brochu-Gaudreau, K., Arsenault, D., Harper, K. & Dubois, C. M. Hypoxia-induced invadopodia formation involves activation of NHE-1 by the p90 ribosomal S6 kinase (p90RSK). *PloS one* **6**, e28851, doi:10.1371/journal.pone.0028851 (2011).

103 Baenke, F., Peck, B., Miess, H. & Schulze, A. Hooked on fat: the role of lipid synthesis in cancer metabolism and tumour development. *Disease models & mechanisms* **6**, 1353-1363, doi:10.1242/dmm.011338 (2013).

104 Cheng, C. *et al.* Glucose-Mediated N-glycosylation of SCAP Is Essential for SREBP-1 Activation and Tumor Growth. *Cancer cell* **28**, 569-581, doi:10.1016/j.ccell.2015.09.021 (2015).

105 Swinnen, J. V. *et al.* Stimulation of tumor-associated fatty acid synthase expression by growth factor activation of the sterol regulatory element-binding protein pathway. *Oncogene* **19**, 5173-5181, doi:10.1038/sj.onc.1203889 (2000).

106 Furuta, E. *et al.* Fatty acid synthase gene is up-regulated by hypoxia via activation of Akt and sterol regulatory element binding protein-1. *Cancer research* **68**, 1003-1011, doi:10.1158/0008-5472.can-07-2489 (2008).

107 Jiang, B. H. *et al.* Phosphatidylinositol 3-kinase signaling controls levels of hypoxia-inducible factor 1. *Cell growth & differentiation : the molecular biology journal of the American Association for Cancer Research* **12**, 363-369 (2001).

108 Luwor, R. B., Lu, Y., Li, X., Mendelsohn, J. & Fan, Z. The antiepidermal growth factor receptor monoclonal antibody cetuximab/C225 reduces hypoxia-inducible factor-1 alpha, leading to transcriptional inhibition of vascular endothelial growth factor expression. *Oncogene* **24**, 4433-4441, doi:10.1038/sj.onc.1208625 (2005).

109 Sang, N. *et al.* MAPK signaling up-regulates the activity of hypoxia-inducible factors by its effects on p300. *The Journal of biological chemistry* **278**, 14013-14019, doi:10.1074/jbc.M209702200 (2003).

110 Zhu, J., Chen, X., Liao, Z., He, C. & Hu, X. TGFBI protein high expression predicts poor prognosis in colorectal cancer patients. *International journal of clinical and experimental pathology* **8**, 702-710 (2015).

111 Thapa, N., Lee, B. H. & Kim, I. S. TGFBIp/betaig-h3 protein: a versatile matrix molecule induced by TGF-beta. *The international journal of biochemistry & cell biology* **39**, 2183-2194, doi:10.1016/j.biocel.2007.06.004 (2007).

112 Bae, J. S. *et al.* Betaig-h3 supports keratinocyte adhesion, migration, and proliferation through alpha3beta1 integrin. *Biochemical and biophysical research communications* **294**, 940-948, doi:10.1016/s0006-291x(02)00576-4 (2002).

113 Kim, J. E. *et al.* Identification of motifs in the fasciclin domains of the transforming growth factor-beta-induced matrix protein betaig-h3 that interact with the alphavbeta5 integrin. *The Journal of biological chemistry* **277**, 46159-46165, doi:10.1074/jbc.M207055200 (2002).

114 Shang, D., Liu, Y., Yang, P., Chen, Y. & Tian, Y. TGFBI-promoted adhesion, migration and invasion of human renal cell carcinoma depends on inactivation of von Hippel-Lindau tumor suppressor. *Urology* **79**, 966.e961-967, doi:10.1016/j.urology.2011.12.011 (2012).

115 McIntyre, R. E., Buczacki, S. J., Arends, M. J. & Adams, D. J. Mouse models of colorectal cancer as preclinical models. *BioEssays : news and reviews in molecular, cellular and developmental biology* **37**, 909-920, doi:10.1002/bies.201500032 (2015).